FIRST MEASUREMENTS OF THE LOW ENERGY TAIL (LET) DOWN TO 0 eV USING AUGER PHOTOELECTRON COINCIDENCE SPECTROSCOPY (APECS) IN Ag (100) AND Cu (100)

by

KARTHIK SHASTRY

Presented to the Faculty of the Graduate School of

The University of Texas at Arlington in Partial Fulfillment

of the Requirements

for the Degree of

MASTER OF SCIENCE IN PHYSICS

THE UNIVERSITY OF TEXAS AT ARLINGTON

DECEMBER 2010

ACKNOWLEDGEMENTS

I would like to convey my sincere gratitude to my research supervisor Dr. Alex Weiss for having faith in me and providing me with all the necessary facilities for the completion of this research. I would like to thank Dr. Ali Koymen and Dr. Suresh Sharma and all the faculty members for their invaluable comments and suggestions. My deepest gratitude to Dr. Hulbert, for hosting my work at National synchrotron Light Source (NSLS), Brookhaven National Labs, Upton New York. It was very good experience to work under his guidance. I would also like to thank Mr. Dong for helping me with my work at the NSLS.

I am highly indebted to Saurabh for motivating me to work at BNL and for being there when I ran into trouble. I would like to Thank Mr. Douglas Coyne for his encouragement and support in this research. This list will not be complete without the mention of some of wonderful colleagues I had- Sushant, Suman, Prasad, and Ajani. Thanks for making my stay here cheerful. Special mention should be made of the wonderful administrative staff in physics- Margie, Amy, Fran, Stacy and Bethany. Thanks for making this our home away from home.

Finally, I would like to thank my family. I express my sincere gratitude to my parents for always believing in me.

November 23, 2010

ABSTRACT

FIRST MEASUREMENTS OF THE LOW ENERGY TAIL (LET) DOWN TO 0 eV USING AUGER PHOTOELECTRON COINCIDENCE SPECTROSCOPY (APECS) IN Ag (100) AND Cu (100)

Karthik Shastry, MS.

The University of Texas at Arlington, 2010

Supervising Professor: Alex H. Weiss

We present measurements in which Auger Photoelectron Coincidence Spectroscopy (APECS) technique was used to obtain the energy distribution spectrum of Ag (100) and Cu (100) over a range of emitted energies from 0 eV to 81eV. These coincidence measurements were successful in separating the low energy Auger lines from a large background, arising from electrons generated through loss processes unrelated to the Auger transition. The measurements revealed a distinct Auger peak at 60 eV for Cu (100) corresponding to the $M_{2,3}VV$ auger transition and an Auger peak at 40 eV for Ag (100) corresponding to the N_2VV transition accompanied by a low energy tail (LET) associated with the Auger transition. The Low Energy Tail (LET) extends to 0 eV and has a broad maximum at ~ 6eV in case of Cu (100) and ~10 eV in case of Ag (100). The integrated intensity of the Low Energy Tail (LET) in Cu and Ag were 6 and 2 times

larger than that of the Auger peak itself respectively. The origin of the LET is discussed in terms of extrinsic mechanisms in which electrons from the peak lose energy as they propagate to the sample surface, as well as intrinsic mechanisms in which multi-electron Auger processes distribute the energy gained by the filling of the core-hole to multiple valence electrons.

TABLE OF CONTENTS

LIST OF ILLUSTRATIONS

CHAPTER 1

OVERVIEW

1.1 Motivation

In this thesis the first measurements of the Low Energy Tail (LET) associated with C VV Auger transitions in Ag (100) and Cu (100) down to 0 eV are reported. The Low Energy Tail (LET) carries vital information about the sample under investigation and constitutes a major portion of a spectrum's spectral weight[1]. Hence it is important to understand the process contributing to the Low Energy Tail (LET) due to the corresponding C VV Auger transitions. In conventional spectroscopic measurements the low energy auger lines are superimposed upon a large background due to secondary electrons which arise due to loss processes unrelated to the Auger process. Auger Photoelectron Coincidence Spectroscopy (APECS) is used to explain the LET due to processes intrinsic to the Auger transition.

X-ray and Auger electron spectroscopy (AES) are the two widely used surface probing techniques. The analysis of the sample under investigation gives us information about the local density of states at the surface, chemical bonding and post collision interaction effects and charge transfer effects[2, 3]. But due to the presence of a large background in the resulting spectrum it is difficult to analyze the raw data. Various numerical techniques can be used to subtract the background, but since they are model dependant it is not possible to eliminate the risk of losing information. Hence it is important to eliminate as much of the unrelated background as possible.

1.2 Introduction

Photoelectron spectroscopy and Auger electron spectroscopy are powerful techniques in probing a sample surface. Photoelectron spectroscopy is used to study the local chemical environments in solids. The analysis of the emission line shape reveals the low energy excitation of the solids, such as phonons, plasmons and electron hole pair. Further investigation of the binding energy of the core photoelectron lines gives information about the local chemical environments of the solids. The Auger spectrum contains chemical specific information about valence band electronic structure. The resulting spectrum from a given sample gives information about the local density of states at the surface, charge transfer effects, chemical bonding, and atomic charge and post collision interaction effects. One of the major challenges encountered for both the techniques is the large background associated with the spectrum. Photoelectron and Auger spectroscopy are closely related as the photoelectron emission is followed by Auger decay for core binding energies less than 1 KeV. Coincidence measurements which combine Photoelectron and Auger spectroscopy techniques allows for substantial elimination of the large background without the loss of valuable data. In coincidence techniques, it is possible to correlate the creation of a core hole of a level with the corresponding subsequent Auger transition. The advent of synchrotrons has made it possible to generate tunable EM radiation ranging from infrared to Ultra violet and soft X-ray regions. The high intensity and tenability of the synchrotron has greatly increased the feasibility of coincidence measurements.

APECS was developed by Haak et al. intended for laboratory x–ray anode use[4]. Experiments to improve the timing resolution were conducted by Thurgate[5, 6]. Later experiments were performed by Jensen et al. on extending the APECS techniques to synchrotron radiation[7]. Weiss et al used APECS to investigate the line shape of the Auger spectra and to study the enhanced sensitivity of oxide surface defects[8, 9]. Various experiments were performed using APECS to probe heavy elements to study intrinsic line shapes and Giant Coster Kronig transitions by Arena, Nangia et al. [10,11] APECS was used in experiments by Sundaramoorthy et al to study the Auger cascade properties and energy broadening in heavy elements [12, 13]. Jensen et al. measured the low energy tail using APECS down to 45 eV and proposed the occurrence of multiple Auger electron emission in Al(111)[14].

1.3 Auger Photoelectron Coincidence Spectroscopy (APECS)

The processes related to Auger Photoelectron Coincidence spectroscopy[15] are illustrated in Fig.1.1. A photon with energy *hv* is incident on a sample knocks out a photoelectron with binding energy (E_c). Due to a hole in the core level, the atom is in an excited state and relaxes by filling the core hole with an electron from the valence band. This process is accomplished by auger electron emission or X ray emission based on the binding energies. Lower binding energies (< 2KeV) mostly relax by auger electron emission and higher binding energies mostly relax by X-ray emission. In coincidence measurements the time difference between the emission of Photoelectron and the auger electrons is ~10^{-15} sec. Hence the photoelectron and the Auger electron are detected in coincidence. The process of emission of a valence electron due to a core electron being knocked out is called CVV Auger decay or Core Valence Valence decay, where E_{v1} and E_{v2} are the binding energies of the valence hole created during the transition and φ is the work function. The kinetic energy of the auger electron is given by

$$KE_{\text{auger electron}} = E_c - E_{v1} - E_{v2} - \varphi$$

The energy of a Photoelectron is given by

$$KE_{\text{photoelectron}} = h\nu - E_c - \varphi$$

The Fig.1.2 shows a conventional image of the Auger Electron Spectroscopy (AES) spectrum of Cu, in which the M VV Auger peak is subdued in the background. The Fig.1.3 shows a comparison of the APECS spectrum with the AES spectrum. The coincidence spectrum represented by the dots show a considerable reduction in the background and a clear Auger peak. This provides us with the necessary insight to understand the competition between intrinsic and extrinsic secondary electrons. The other advantage of APECS is the ability to distinguish the Auger spectra with origins different from one to another. Previous experiments have demonstrated that APECS can distinguish between surface and bulk atoms and differentiate between atoms in metal oxides and metals. APECS is known for its high surface selectivity and its ability to eliminate the core-hole lifetime to the auger and photoelectron line shapes.

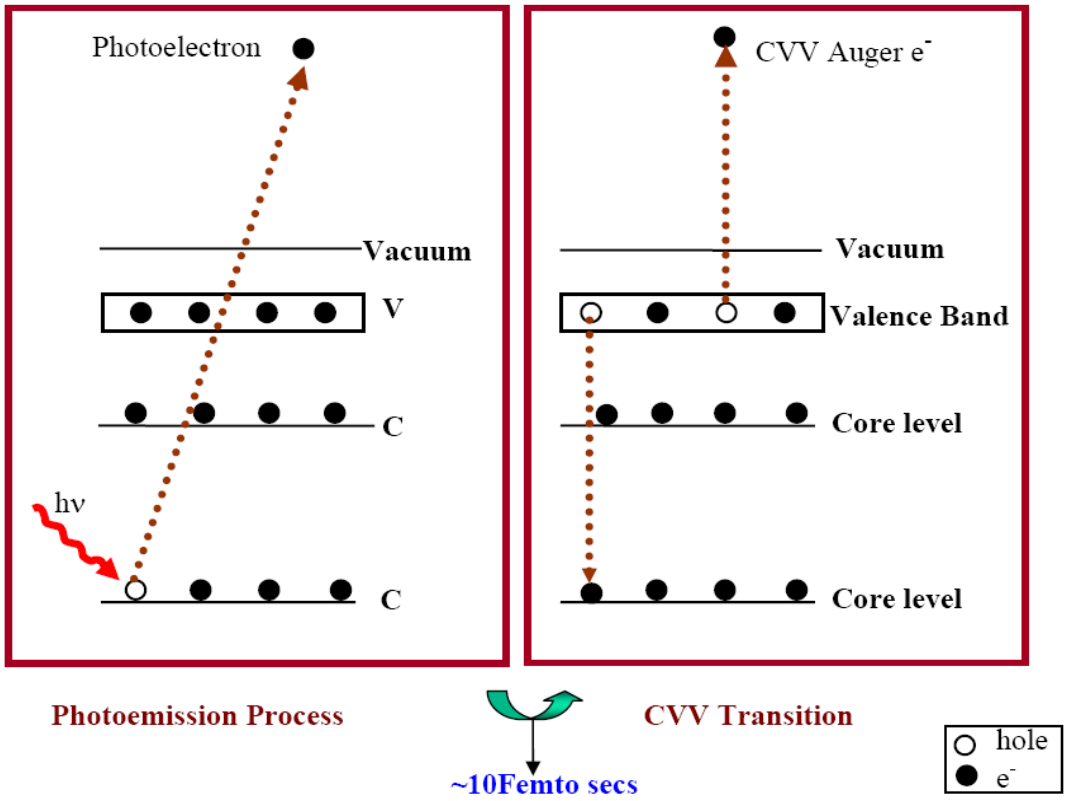

Fig. 1.1 Photo ionization followed by the auger transition from the valence band, which is the process involved in APECS[16]

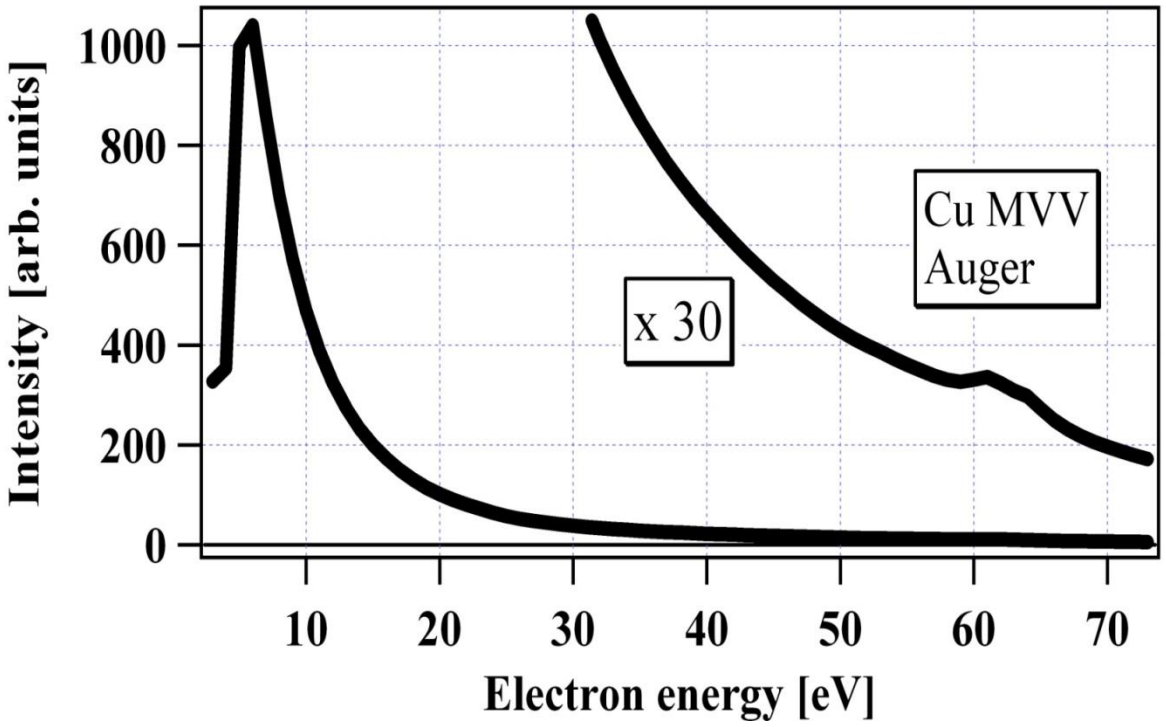

Fig. 1.2 Auger electron Spectrum for an M VV transition in a Cu sample. The M VV notation refers to the hole created in the M (shell) and VV is the valence electrons involved in the transition. The Auger peak at 60 eV is hardly visible, only on magnifying it by 30 times is the Auger peak visible

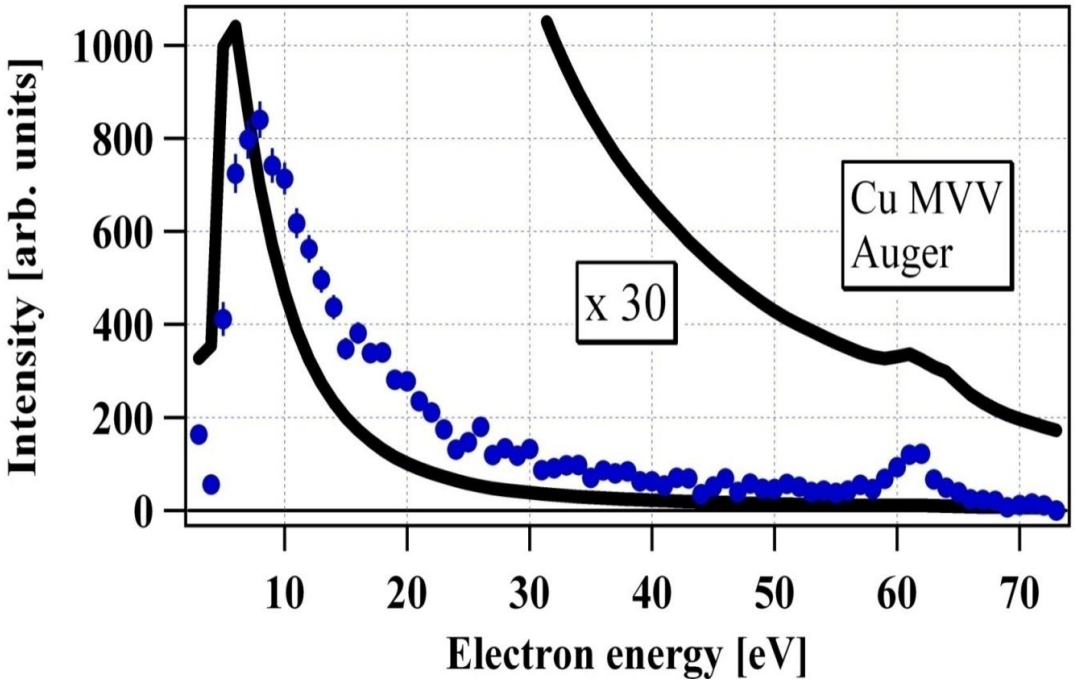

Fig. 1.3 Comparison between an Auger electron Spectroscopy (AES) and Auger Photoelectron Coincidence Spectroscopy (APECS). The black line represents the AES spectrum and the blue dots are the APECS spectrum. The auger peak is a clearly visible at 60 eV in case of APECS

1.4 Low energy Tail

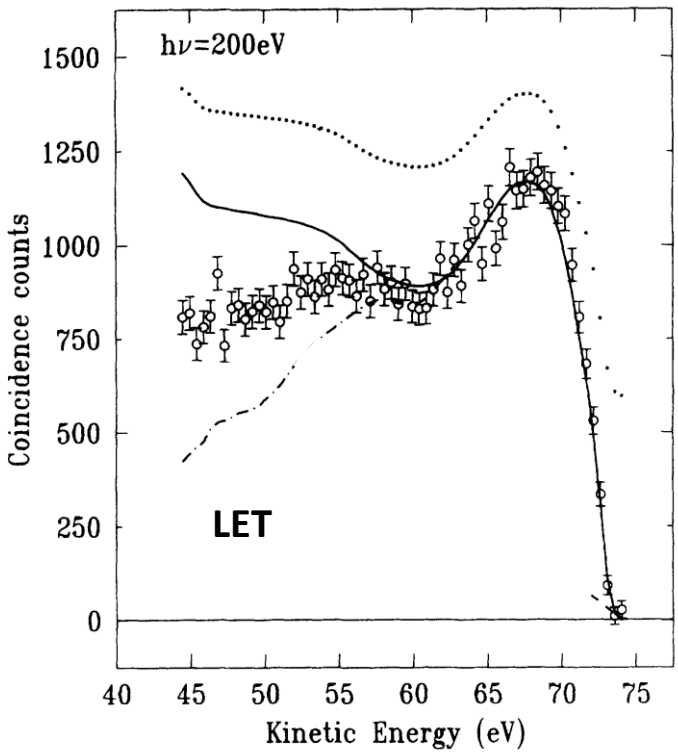

Fig. 1.4 shows the singles and coincidence spectra of Al (111) incident by a beam of photons of energy 220 eV (Ref 14, Jensen et.al, PRL Vol. 45, No. 23).

Since the main focus is on the various processes that generate electrons in the Low energy side of the spectrum. It is therefore important that we define what we mean by "Low Energy Tail". The Low Energy region of the spectrum below the Auger peak is termed as the "Low energy Tail". The Fig.1.4 depicts the measurement made by Jensen et.al on Al (111). The Al (111) $L_{2,3}$ VV Auger spectrum was taken at 200 eV photon energy. The dotted line is the singles spectrum referenced to zero counts. The circles are the coincidence spectrum with the fixed analyzer at 127 eV, the 2p photoelectron peak is observed at 68 eV. The solid line is the singles spectrum with a constant background subtracted from it. The coincidence spectrum (circles) and the constant background subtracted singles (solid line) are normalized to the same height at 68 eV. The dotted dashed line is the coincidence spectrum minus the difference between the singles (solid line) and coincidence spectrum (circles). The dotted dashed line is intended to estimate the

contribution of low energy electrons due to processes intrinsic to the Auger transition. The LET was measured only down to 45 eV in Jensen's experiment. In this thesis we measure the Low Energy Tail (LET) down to 0 eV and estimate the contributions in terms of intrinsic and extrinsic processes to the Auger transition. It is therefore paramount that we investigate the question of whether the LET increases, decreases or is constant, when the Low Energy Tail is measured down to 0 eV, as shown schematically in Fig.1.5.

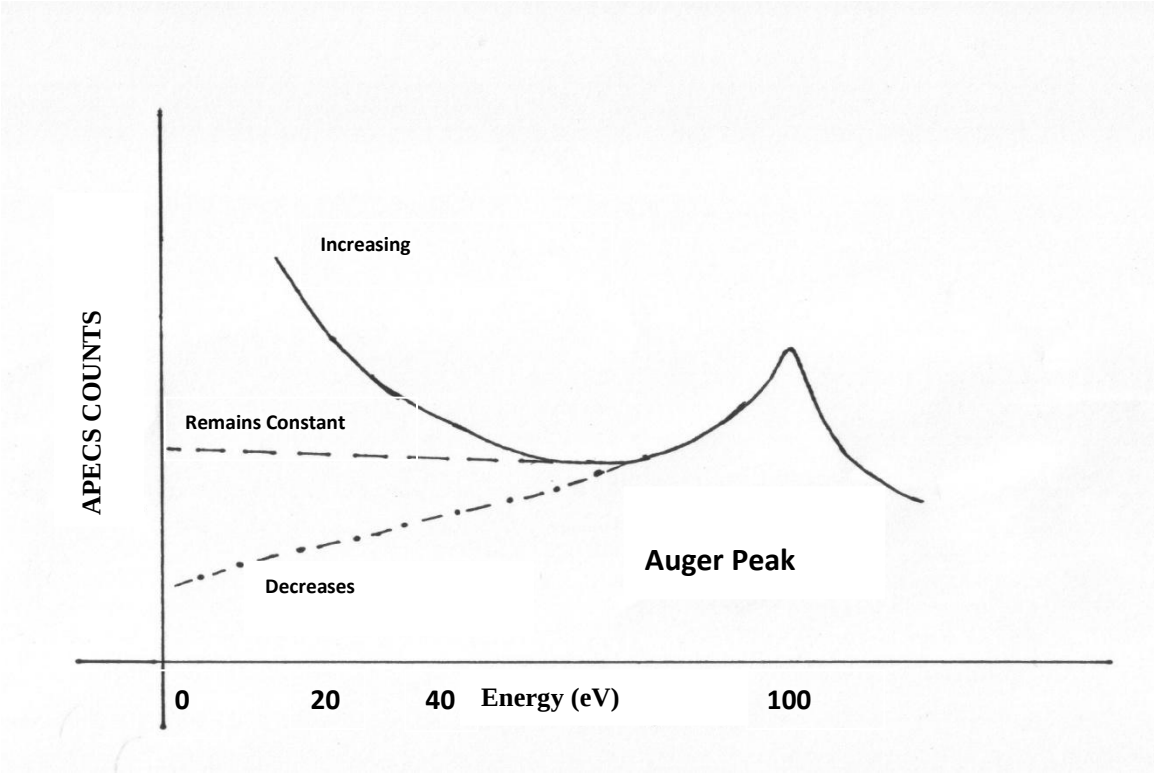

Fig. 1.5 is a cartoon of an APECS spectrum depicting whether the LET increases (solid line), decreases (dash-dotted line) or is constant (dashed line).

This thesis is arranged in 4 chapters. Chapter 1 talks about the fundamentals of Auger Photoelectron coincidence spectroscopy (APECS) and Positron annihilation induced auger electron spectroscopy (PAES) mechanisms are discussed. Chapter 2 presents the experimental setup of the APECS experiments carried out at Brookhaven national Labs (BNL). Chapter 3 presents the results of the APEC measurements on Cu (100) and Ag (100) respectively in detail. Chapter 4 presents a brief summary of the thesis results.

CHAPTER 2

EXPERIMENT DETAILS

Initial core level spectroscopy measurements were done using conventional x-ray tubes. These sources can generate flux in the hard x-ray region (2-100 KeV) but little in the soft x-ray (0.5-2 KeV) [17,18]. Since the advent of high flux tunable synchrotron sources, it has been possible to achieve better resolution and more surface selective experiments as the energies can be scanned over a wider spectrum. The experiments reported in this thesis were carried out at U1A beam line of the National Synchrotron Light Source (NSLS) at Brookhaven National Lab (BNL), New York.

2.1 NSLS storage ring

The NSLS is a Department of Energy (DOE) funded research facility in Brookhaven National Labs at Upton in New York. The NSLS has two beam lines, one producing intense VUV and the other producing X-ray light. The floor plan is depicted in Fig.2.1. The VUV ring produces radiation in the range from dedicated primarily to research in surface science. The electrons for the VUV and X-ray beam lines are generated by a 750 MeV booster synchrotron. The several stages involved in the generation of the electrons are explained in the following paragraphs.

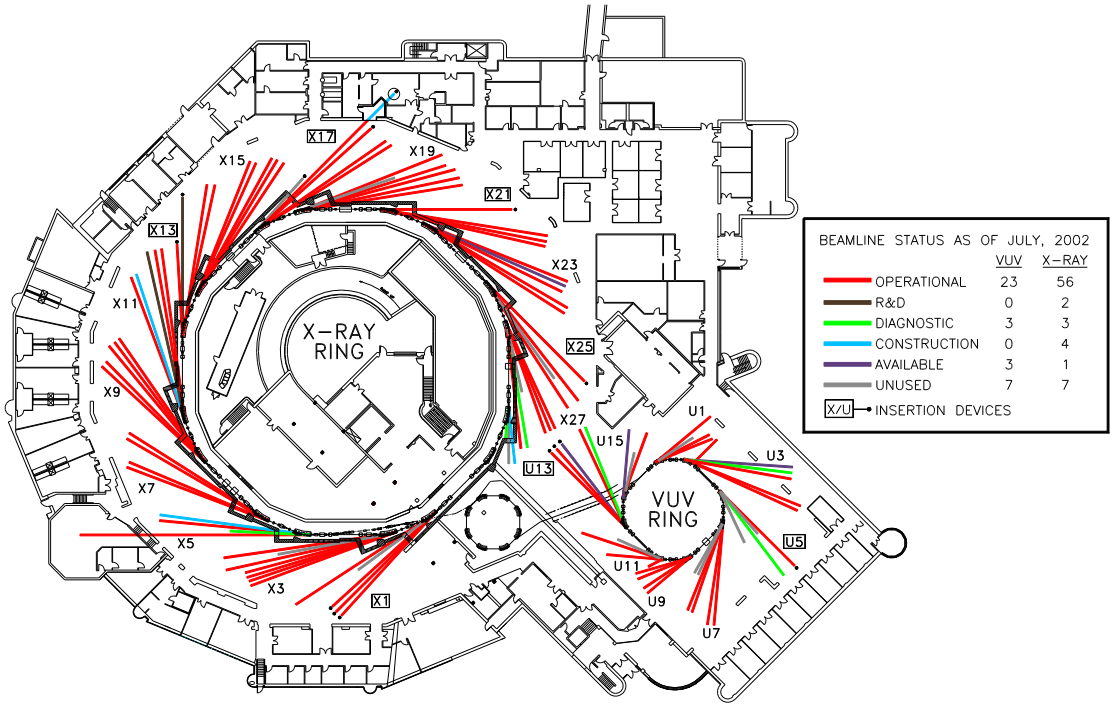

Fig. 2.1 Floor Plan of the X- ray and VUV- ring at theNational Synchrotron Light Source (NSLS), Brookhaven National Labs[20]

The NSLS linear accelerator (LINAC) consists of a series of an electron gun, an accelerating cavity also known as the Low Energy Beam Transport System (LEBT), a RF system and a beam transport system. The electrons are generated in bunches by the electron gun. The electrons are now bunched and are prepared for optimum injection and capture in the LINAC while passing through the low energy beam transport to the booster ring. A LINAC now accelerates the beam of bunched electrons to 120 MeV. Now, a bunch of RF fields at roughly 2700MHz accelerate the beam from 100 KeV to 116 MeV. In order to minimize the radiation resulting from the rejected electrons, quadrupole magnets are used to focus and guide the beam in the horizontal and the vertical directions. Dipole magnets are employed to bend the beam around the corners. The beam is now focused and hence can be injected into the booster ring. Finally a RF cavity raises the energy of the beam of electrons to 750 MeV. When the maximum energy is reached the beam is fed into the VUV and X-ray beam lines respectively. In the case of the VUV beamline, the electron bunches are shunted by magnets in the VUV storage lines. Here, up to 9 electron bunches orbit the ring at 800 MeV which is the desired operating energy[20]. The beam is now fed into the VUV ring after the injecting system is turned off. The orbit is maintained by eight dipole magnets that bend the beam around the corners. At every bend in the ring, the electrons lose energy mainly in the form of Ultraviolet (UV) light. The energy that is lost due to this is giving back to the beam by radio frequency cavities which operate at roughly 50 MHz The UV light can be accessed at the respective end stations by opening the photon shutters connected to the VUV ring.

Similar to the VUV ring, the X-ray ring is also filled. The electron bunches are injected into the LINAC and accelerated in the booster ring to 750 MeV. In the X-ray ring there are up to 30 bunches of electrons orbiting with 750 MeV. Once the X-ray ring is filled to the operating current, the radio frequency increases the energy to 2.8 GeV. There are sixteen dipole magnets that bend the beam around the closed orbit. The X-ray light can be accessed at the respective end stations by opening the photon shutters connected to the X-ray ring.

The APECS experiment detailed in this thesis were performed at U1A beamline at the National Synchrotron Light Source (NSLS) at Brookhaven national laboratory. The VUV storage ring functions at 800 MeV with a beam current of ~1000mA. Out of the 9 bunches or "buckets" of electrons orbiting the ring, 7 are consecutive bunches/ buckets filled and the last two are empty. The orbital period of the electrons around the storage ring is 170 ns. The time interval between two consecutive bunches is approximately 19.2 ns. There are 16 beamlines in the VUV ring dedicated to various kinds of research which require energies in the UV regime. Similarly the X-ray storage ring at the NSLS functions at 2.8 GeV with a maximum beam current of approximately 300mA. Of the 30 bunches/buckets of electrons 25 are consecutive bunches filled and the rest empty. The lifetime of the beam is approximately 20 hours. The orbital period for a bunch of electrons around the ring once is 567.2ns. The time interval between two consecutive bunches is approximately 18.9 ns. There are 61 beamlines in the X-ray ring dedicated to various kinds of research which require energies in the X-ray regime.

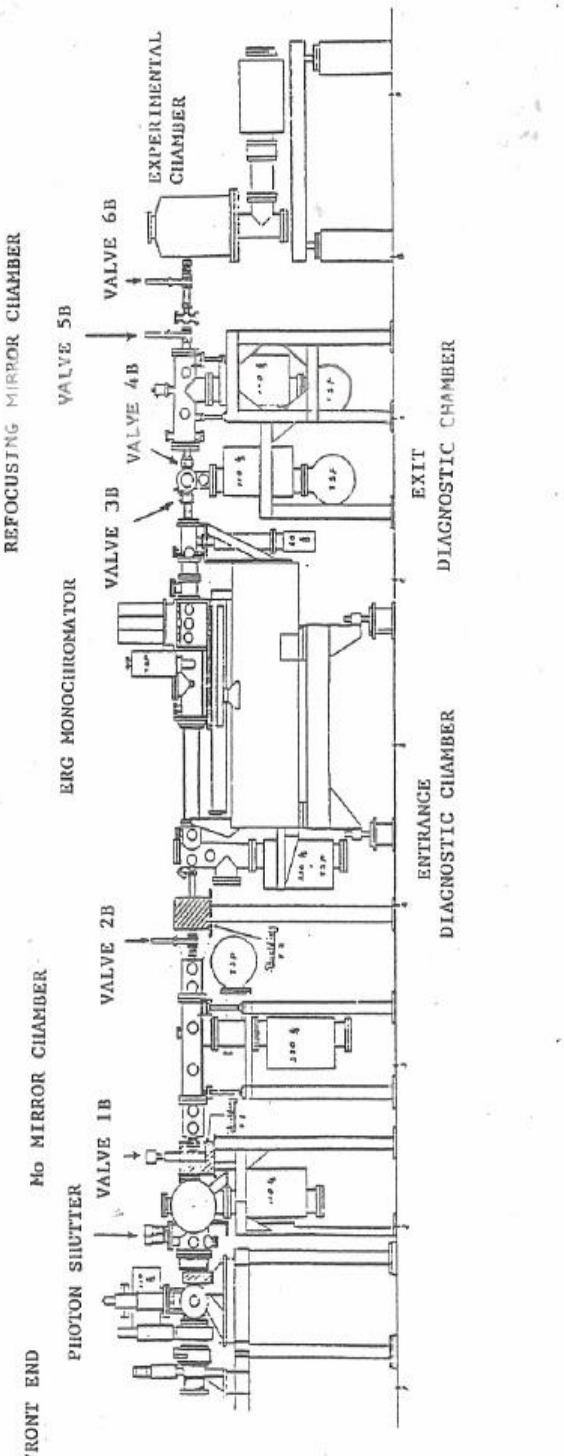

Fig. 2.2 Schematic view of the U1A beamline, NSLS at BNL[16] (Ref 16, R. Sundaramoorthy, thesis, 2007)

2.2 Beamline Details

The U1A beam line consists of optics and other necessary accessories for directing the photons into the end station. A computer control system is used to select the energy of photons that are directed onto the sample from the UV storage ring. Fig.2.2 is the schematic diagram of the U1A beamline.

The main component of the U1A beam optics is the ERG monochromator, which was designed by F.C. Brown and S.L. Hulbert[21]. A computer controls the range of photon energies that are directed onto the sample from the UV storage ring.

The components constituting the U1A beamline are

a) The sample chamber.

b) Refocusing mirror.

c) ERG monochromator.

d) Horizontal focusing mirror.

2.2.1 The ERG Monochromator

It is used to guide and focus the photon beam to the sample. Its primary function is to focus and transmit a single wavelength of the photon beam in the vertical plane. It consists of mirrors M_1, M_2 and gratings G_1, G_2 as its components. A 30 cm long gold coated elliptical mirror is located at a fixed distance of about 52 cm from the entrance slit S_1. The width of the entrance and exit slit can be varied and is used to focus the photons as a horizontal beam; this allows the monochromator resolution to be adjusted. The photon beam is then made incident on one of the gratings G_1, G_2, G_3 which have a radius of curvature 2m, 3.7m, 5m and each has600 to 1200 lines per mm [27]. Rowland geometry is used as a basis for the scanning of energies by the monochromator.

The positions of the gratings and the movement of the beamline optics are taken care of by a system of four stepper motors accompanied by mechanical limit switches. The stepper motors are controlled by a motion

controller which also allows continuous scanning of the wavelength of the resulting monochromatic light. The software program 'Un' controls the monochromator and records the input of data into the computer[22]. A detailed figure of the complete beam line setup is shown below for our better understanding of the components involved.

2.2.2 UHV Chamber

It is paramount that pressure of the order of 10^{-10} Torr be maintained in the beam line for successful surface analysis. This range of pressure is called ultra high vacuum (UHV). Such low pressures are obtained by using a series of mechanical, turbo molecular and ion pumps in the chamber. The following paragraphs will explain in detail the various pumps employed in maintaining consistent vacuum.

Since the VUV ring is shared by multiple end stations extreme care has to be taken so as to not destroy the vacuum in the storage ring due to any negligence at the end station. Hence differential pumping is used to maintain optimum vacuum at the VUV ring even if there is a loss of vacuum at the end station. The minimum vacuum required to open the end station to the VUV ring is in the range of 10^{-9} to 10^{-10} Torr. To achieve this, it is not possible to pump the chamber down to UHV pressures by using a single pump. We begin by pumping the chamber down to 10^{-4} Torr. A rotary vane mechanical pump (Varian SD-90) and a turbo molecular pump [Pfeiffer TPU-050 (50- L/S)] is used to pump the system down to 10^{-6} Torr. Then an ion pump [Perkin-Elmer Model # 2070122(120 L/S)] along with a Ti sublimator combination pumps the chamber down to pressures of the order of 10^{-10} Torr. There are a series of valves in the beamline in order to open the chamber to the incoming photon beam. The valves 1B and 2B separate the M_0 mirror chamber from the beamline. The valves 2B and 3B separate the monochromator, the valves 3B and 4B isolate the refocusing mirror, and the valve 6B isolates the sample chamber from the rest of the beamline. The valves 5B and 6B ensure that there is no leakage of gas into the VUV ring from the sample chamber. In addition to the valves mentioned above, there are interlock valves and safety shutters which help as a safety measure to protect the ring vacuum[27]. The Fig.2.2 depicts the complete diagram of the U1A beam line for our better understanding.

The sample chamber is on wheels can be shifted to different beamlines if necessary to accommodate NSLS beamline availability. The APECS sample chamber was attached to the U1A beamline prior to performing

the experiment. The UHV vacuum in the sample chamber is established by using a mechanical, a turbo molecular pump, an ion pump and by overnight baking. It has view ports and a sample manipulator which holds the sample in place. The chamber is also equipped with leak valves that let Argon and Oxygen into the chamber for sputtering and oxidization of the sample respectively. The chamber is equipped with a sputter ion gun for cleaning the sample surface. Two cylindrical mirror analyzers (CMA) the key components of the coincidence system are aligned at 145^0 from each other at 10^0 below the horizontal.

The sample manipulator has 4 degrees of freedom enabling us to move the sample in (x, y, z, ɵ) as per our requirements. The position of the sample is changed from its data taking position during sputtering procedures. The whole UHV chamber is on an adjustable mount in order to align the sample, the stationary cylindrical analyzers in the best possible alignment with respect to the incoming photon beam from the VUV ring. The second cylindrical mirror analyzer is fixed on its own adjustable mount. The whole alignment of the various components of the system is critical and important for achieving optimum count rate.

2.3 U1A Electronics

The following sections discuss in detail the various electronic components employed for data assimilation at the U1A beamline.

2.3.1 CAMAC CRATE Electronics

The controls of the whole U1A beam line are managed by a computer. The interface electronics for the end station is housed in the CAMAC crate (1502). The CAMAC crate is a vital component of the system as it coordinates the U1A computer and the designated electronics. The computer not only talks to the CAMAC crate but also controls the ERG monochromator. The modules installed in the CAMAC crate include D/A converter, Quad Scalars (left, right), two real time clocks, NIM/TTL converter, V-F converter. The Fig.2.3 shows the schematics of the connections and the interface electronics in the CAMAC crate.

D/A converter: The primary function of the D/A converter is to set the energies on the fixed and scanning analyzers. A 16- bit digital input number id converted to an analog ramp signal. A display unit mounted on

the circuit board displays the voltages on the respective analyzers. The fixed analyzer is set to the desired photoelectron peak. The voltage on the scanning analyzer is scanned through the spectral regions of interest.

Real time Clock: In brief, the Real time clock (DSP RTC018) accepts a command from the U1A computer. The command specifies the dwell time and generates a gate signal which is used to define the counting interval of the (QS – 450) quad scalar. The signal generated by the Real Time Clock is a gate signal precisely equivalent to 21/8 * dwell time) seconds.

Quad V-F converter: A SLS – 60440 Quad V-F converter is used to convert voltage signals into signals proportional to the input voltages. The resulting output voltage is sent to a TTl-NIM converter and then to a Quad Scalar.

Quad Scalar (left): Is a DSP- QS- 450-4 channel Counter which has 4 inputs and 4 gates. The gate receives signals from the DSP RTC 018 real time clock, which acts as a timer to start and stop the counting. The start is specified by the clock and is counted till the pulse goes down to zero. The quad scalar accepts two inputs for the photoemission counts from the constant fraction discriminators (CFD'S) and two inputs from the MCA for the coincidence counts.

Quad Scalar (right): The DSP-QS-450-4 Quad scalar has 4 inputs and 4 gates of which only two are used. An analog signal proportional to the ring current is sent to the first channel of the V/F converter thereby generating a TTL signal whose frequency is proportional to the ring current. The photo current signal generated at the exit slit of the monochromator is sent to the second channel of the V-F converter.

TTl-NIM converter: is employed to convert the TTL signals to the NIM standard signals accepted by the Quad Scalars. Signals such as beam current, true + accidental coincidence and accidental coincidence signals from the PHA and the photoemission counts from the CMA's constitute the TTL signals.

Counting Electronics: the signals from the left and right CMAs are converted to NIM signal after amplification and fed to the Quad Scalar counters which take the signals from the real time clock. The NIM converted coincidence signals are fed into the quad scalar and gated by the signal from RTC 018. The

output of the V-F signals proportional to the mesh and beam current are fed to a third party scalar which has a real time clock to gate the pulse community.

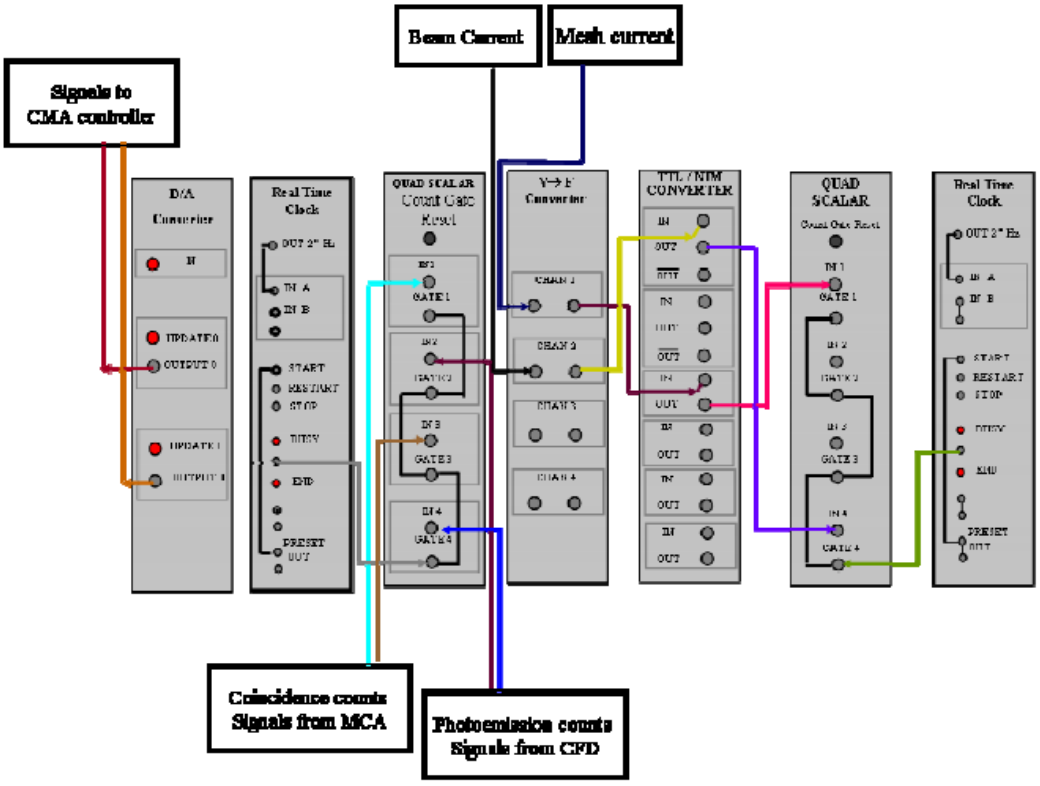

Fig. 2.3 Schematic diagram of the signal paths among the modules used for counting[16] (Ref 16, R. Sundaramoorthy, thesis, 2007)

2.3.2 Coincidence Electronics

The output of both the CMA's is directed to an amplifier and a discriminator. The output signal from the discriminator and the amplifier of one CMA is used as the start signal of a TAC time to amplitude converter. The signal form the second CMA which too is discriminated and amplified is sent to the delay so that the data is in the positive regime. This signal is used as the stop signal to the TAC. The analog output

signal of the TAC is proportional to the start and stop pulses, the MCA performs a pulse height analysis and records the results as a histogram. The configuration of the coincidence electronics at the U1A beamline is shown in Fig.2.4. A detailed explanation of the individual components used is given in the following paragraphs.

AMPLIFIER: To amplify the fast photomultiplier type signals, we use a Model 612 AM which is a 6 channel NIM module. There are 6 channels of the 612 AM of which each one of them use two internal amplifiers to achieve a variable gain up to 40x.

CFD: (Constant Fraction Discriminator): to minimize the timing "walk" due to the pulse height variations we employ a CFD. The CFD can differentiate between noise and data pulse by setting a pulse level below which pulses are rejected. The pulses from a channeltron have a distribution of amplitudes but the same rise time. Since, the pulses have in general different pulse heights. A discriminator that fires at a fixed voltage would produce output pulses come out at different times relative, to the peak of the pulse. By firing at a constant fraction of the peak, pulses of the same rise time will produce output pulses at the same time relative to peak, independent of the pulse height.

Delay: For the coincidence experiment a delay of 500 ns is required. The delay unit used is an ORTEC model 425A nano second delay unit. It provides a delay for a signal in 1 ns steps of 0 to 63 ns. Here, we use two delay units in series to achieve the desired delay for the current experiment. The effective delay time introduced is 126 ns. The cable adds an intrinsic delay of 1 ns per foot.

TAC (Time to Amplitude Converter): To measure the time interval between pulses to its start and stop inputs and generates an analog output which is proportional to the measured time. The TAC output is a pulse of height proportional to the time difference between the start and stop. Typically, the output of the low energy electrons is connected to the start of the TAC. The output from the higher energy electrons delayed by 123 ns and the intrinsic delay is the stop of the TAC. Hence, the auger signal is the start and photoelectron is the stop.

MCA/PHA (Micro Channel Analyzer/Pulse Height Analyzer): The model used is TRACOR NORTHERN TN7200. The PHA displays the spectra of counts in form of a histogram as a function of time. The PHA gets its input from the TAC. The output form a TAC is a pulse in the range of 0-10 V. The total number of channels 1024 is divided equally among 500 ns, which is the input range of TN-7200. The incoming TAC pulse is converted into counting pulses of a particular height, the voltage of the pulse the corresponding counts are put in a particular channel. There are 9 different memory registers that can be used.

Rate Meter: The rate meter modules (NIM) are used to monitor the count rates when aligning the sample with respect to the beam and when checking for the overlap of the two CMA's. It gives the number of counts coming from the channeltron. It is also used to measure the approximate value of the counts in the fixed spectrum. The alignment of the CMAs is paramount, since the degree to which the two analyzers image the same volume directly determines the maximum achievable effective count rate. The rate meters are important in aligning the two analyzers to get maximum efficiency.

ROI (Region of Interest): Two regions of interest, (ROI), were set in the MCA; ROI (C) corresponds to the region which has counts that comprise of trues and accidentals and ROI (A) corresponds to the region which has counts that comprise only of accidentals alone. A image of the ROI (0) and ROI (1) is shown in the Fig.2.5.

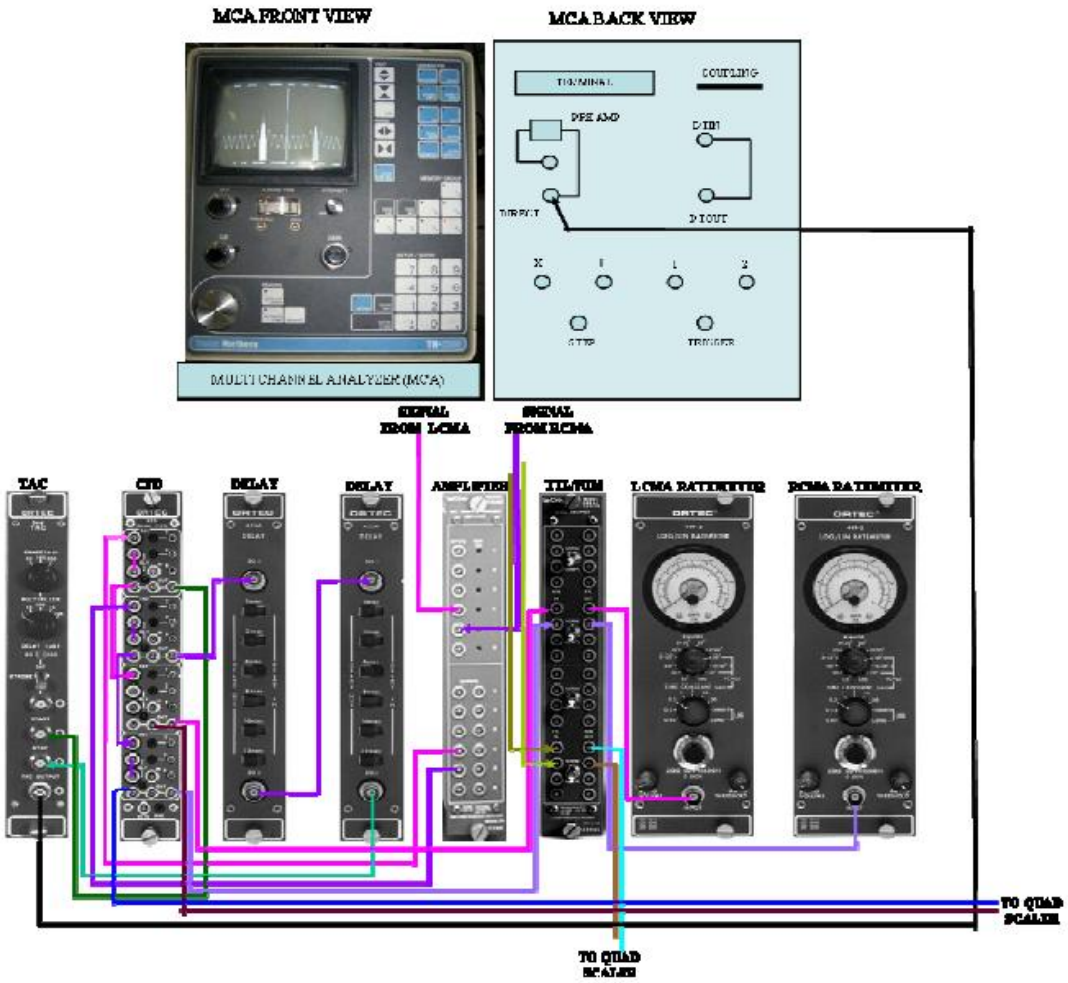

Fig. 2.4 Circuit diagram of the Coincidence electronics[16] (Ref 16, R. Sundaramoorthy, thesis, 2007)

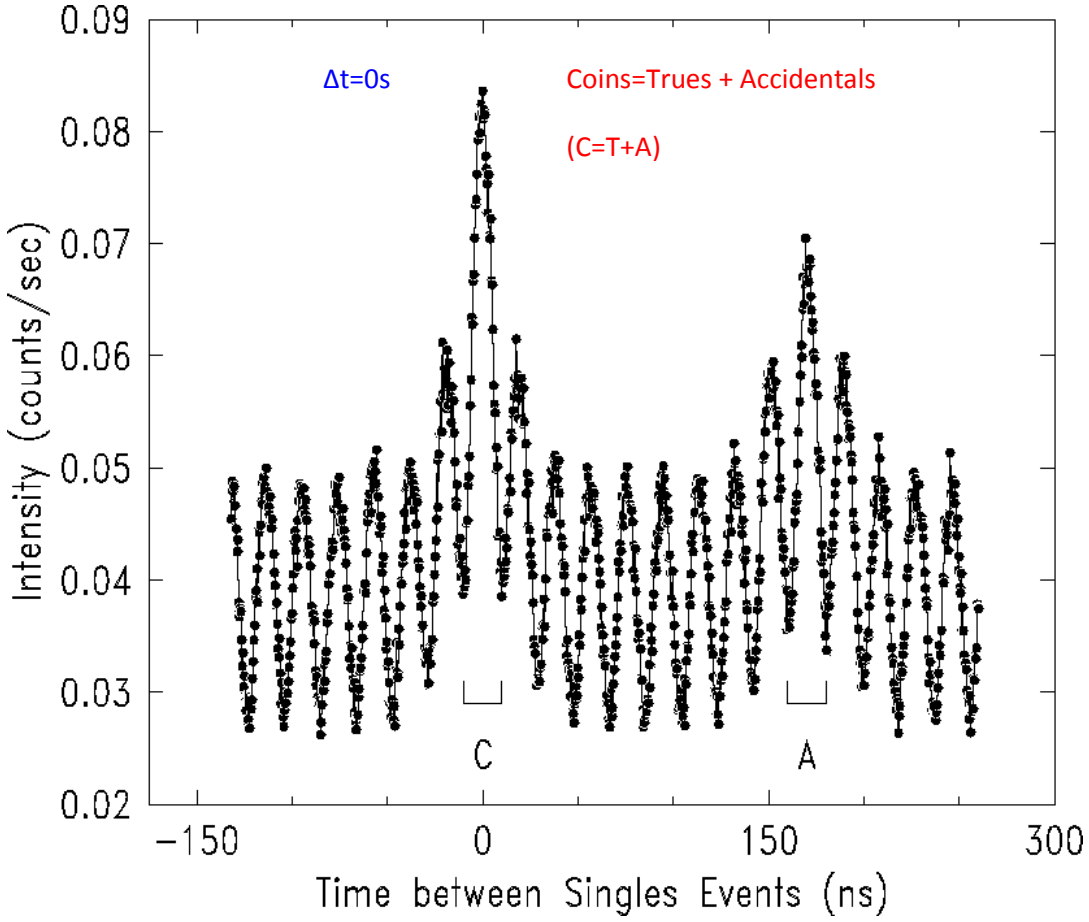

Fig. 2.5 Pulse height analysis of the TAC output. Showing the structure of the synchrotron bunch'. The Region of interest (ROI) marked C is the Trues + Accidentals, the region marked A is only the Accidentals[16] (Ref 16, R. Sundaramoorthy, thesis, 2007)

2.4 Timing electronics

The electrons in the synchrotron go around in time bunches and hence the data has the same timing structure as the synchrotron bunches. The typical spectrum is shown in the Fig.2.6. There are two main peaks taller than the rest. The peak with ΔT=0 is the coincidence peak 'C', this peak is due to the electrons detected at the CMAs at the same time, 15 ns resulting from the photons of the same bunch. The second large peak corresponds to electrons detected in CMA, after the bunch has travelled once around the ring

(i.e.) with a time difference of 170 ns. The peak is due to photons from different pulses. This is the accidents peak ‘A’. The peak at ΔT= 0 ns has contributions from the coincidence and the accidentals combined, the peak at ΔT= 170 ns has contributions from accidentals alone. ‘ΔT” can be explained as the time difference between electrons entering the CMA 1 and CMA 2. The width of the peak can be manipulated (i.e.) broadened by timing resolution of the CMAs; a small contribution to the width of the electron bunches in the ring, timing contributions from the electron modules. There are total of nine peaks between the coincidence peak at ΔT= 0 ns time and the accidents peak at 170 ns. Considerations of the bunch structure used to explain the observations of the accidental intensities as 7/9, 6/9, 5/9, 5/9, 5/9, 5/9, 5/9, 5/9, 5/9, 6/9, 7/9 etc.

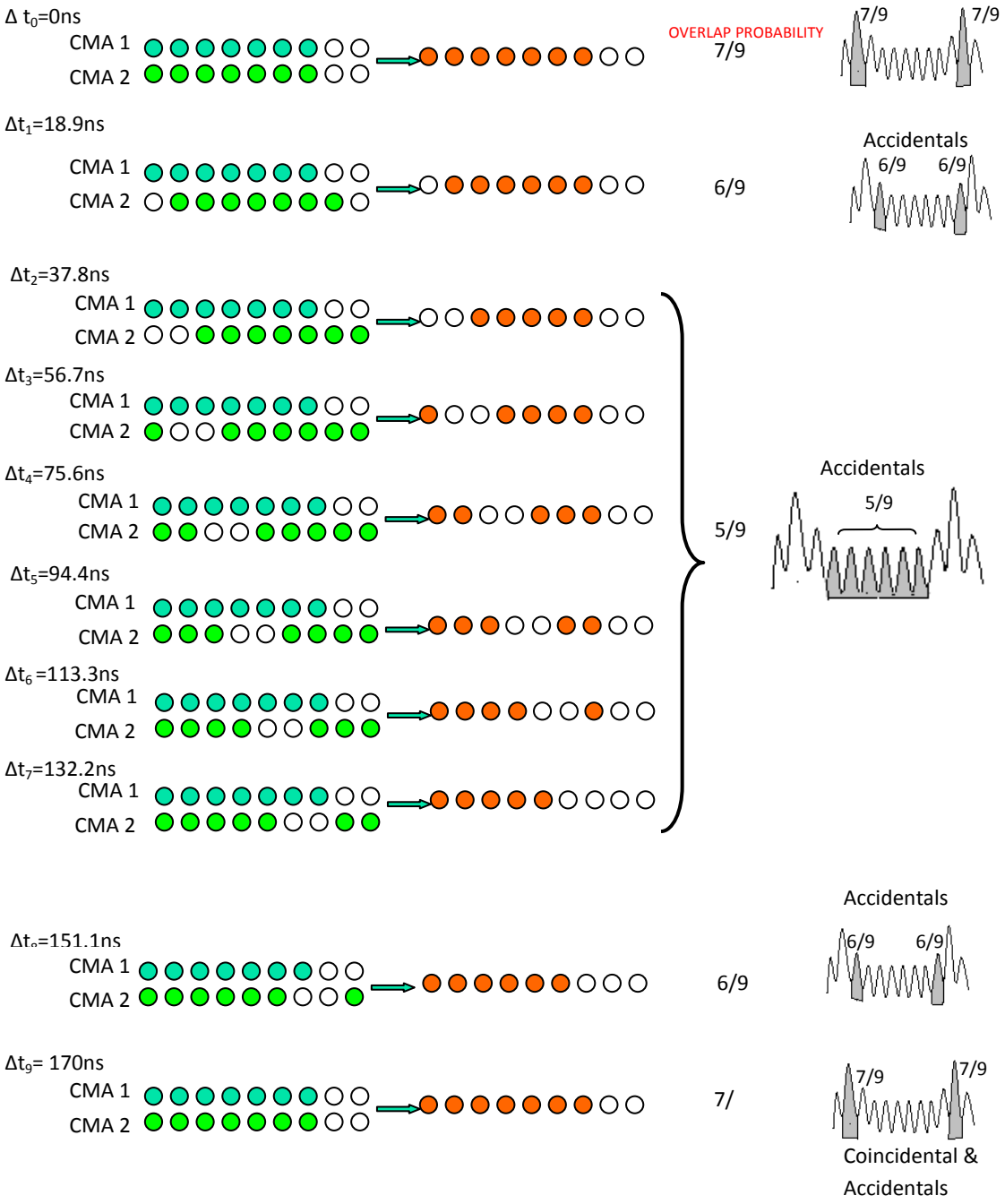

Fig. 2.6 Timing spectra, depicting the overlap of empty photon bunches with filled bunches (Ref 16, R. Sundaramoorthy, thesis, 2007)

2.5 Cylindrical Mirror Analyzer

The Fig.2.7 depicts the electronics used to set the voltages on Inner Cylinder (IC) and Outer Cylinder (OC). The following sections will deal with the power supplies and the controller employed in operating the cylindrical mirror analyzer.

Extra Power Supply: The extra power supply is used to boost the voltage from the pass energy divider. The output of CMA's from the computer controlled power supply is enough to scan up to 500 eV. In metals of interest, the Kinetic energy may range over 1 keV and hence more than one power supply may have to be used.

PASS Energy/ Voltage Divider: The pass energy/ voltage divider is used to set the pass energy, decides the energy of the electrons that can pass through the CMA to be detected. The CMA's Inner Cylinder (IC) and the Outer Cylinder (OC) are set in such a way that the electron with Kinetic energy equivalent to the pass energy can reach the channeltron. The inner cylinder is more positive than the outer cylinder.

AES supply: The voltages to the channeltron are set at 2.3 KV and 2.36 KV for the LCMA and RCMA respectively. The AES lead is connected to the AES connectors of the CMA's which acts as the collector bias.

Offset Supply: This supply gives an output (0-500 V DC) linearly proportional to the 0-10 V DC input from CAMAC D/A module. It has two programmable power supplies, to set the voltages on the CMA's that determine the energies of electrons to pass through them. These voltages are often termed as ramp voltages and are denoted as V_{ramp}. There is a panel on the front that indicates the voltages on the CMA's.

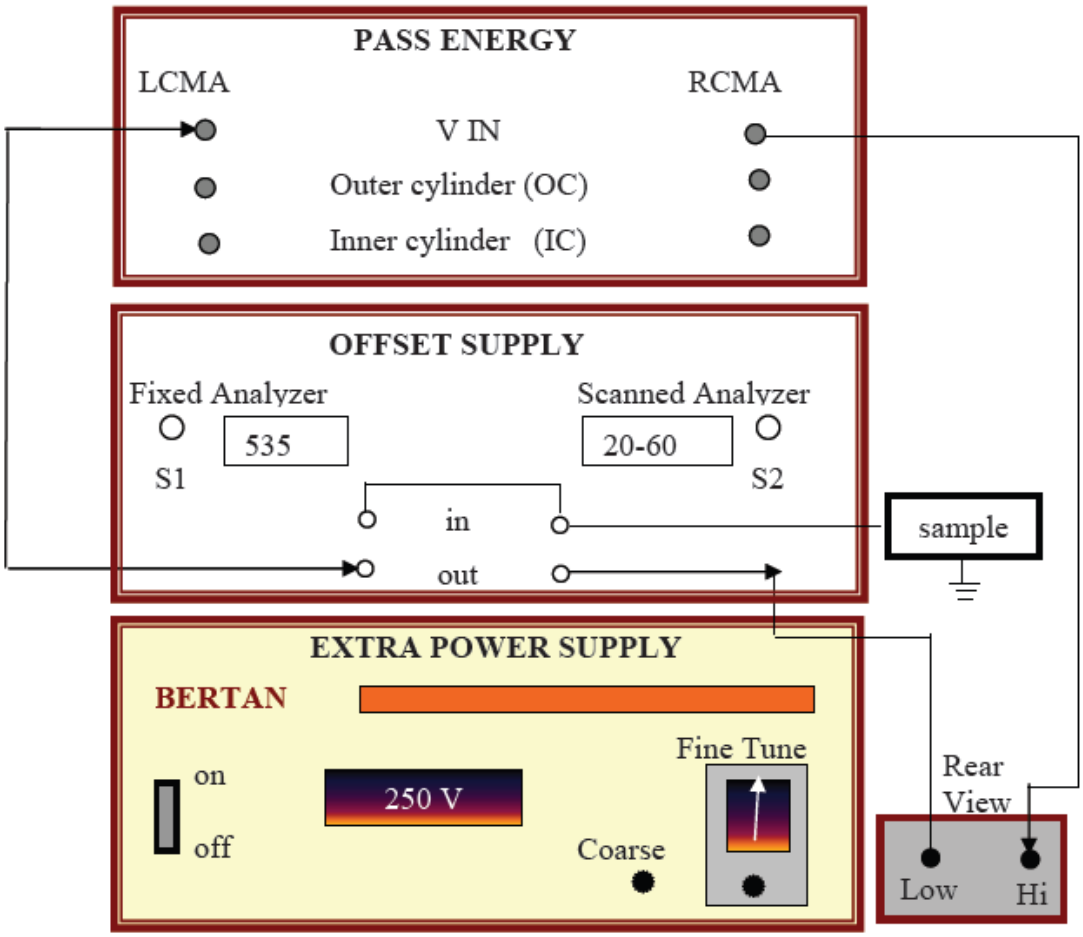

Fig. 2.7 Schematic diagram of the power supplies used to set the voltages on the inner and outer cylinder[24]

2.5.1 CMA Components

CMA: the chamber houses 2 double pass cylindrical mirror electron energy analyzers (PHI Model 15-255G). The two 8- inch ports that house the two CMA's are oriented at 145^{o} from one another in a horizontal plane 10^{o} below the horizontal on the chamber. The CMAs consists of two concentric coaxial cylindrical metal cylinders, namely the inner cylinder (IC) and the outer cylinder (OC). To allow the electrons in and out of the region between the cylinders, the inner cylinder is equipped with grid covered apertures. The Fig.2.8 illustrates the controls and connections of the CMA.

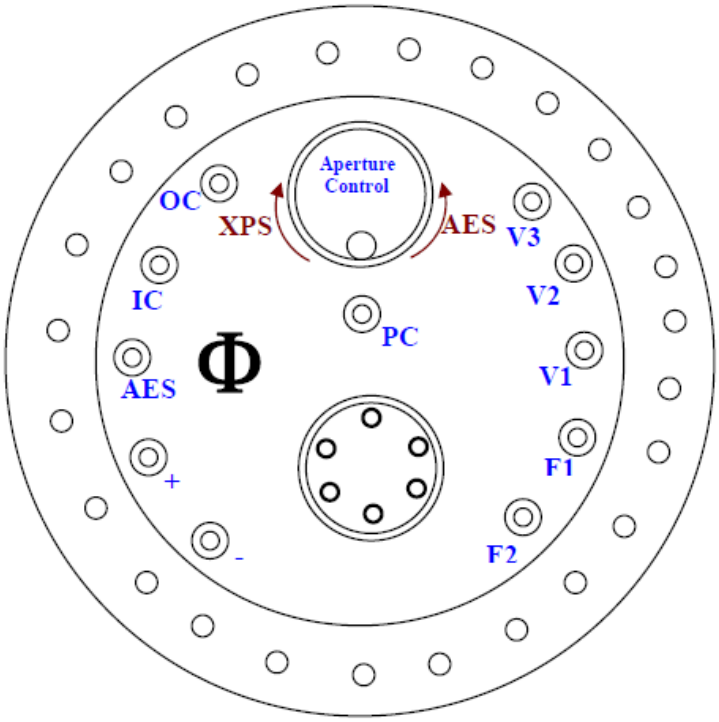

Fig. 2.8 Flange-mounted terminals on the PHI model 15-225G Precision electron energy analyzer[24]

The basic components of a CMA are

1) Channeltron(electron multiplier).
2) Double Pass Cylindrical Mirror Analyzer.
3) Variable aperture system.
4) Retardation Grid.
5) Internal Electron Gun.
6) Deflection Plates.

The internal apertures of the CMA can be chanelled from small to large by the rotating knob on the back of the flange of the CMA. For accurately measuring the kinetic energy of the electrons ejected from the sample, it is essential proper distance be maintained. The distance maintained for this model of CMA is approximately 28 cms. The internal electron gun is not used, as photons from the NSLS storage ring.

When a beam of photons from a storage ring hit the sample, a large number of electrons are expelled at different energies and angles. The CMA's can detect only those electrons expelled at angles of $48^{o} \pm 5^{o}$ relative to the CMA axis. The basic construction of the CMA involves two coaxially placed cylinders with a small dist between them. The outer cylinder is negatively biased than the inner cylinder. The electrons entering the analyzer from the sample now are deflected towards the axis of both the cylinders. The energy of the electron is a direct measure of its kinetic energy, hence, the faster moving electrons impinge on the outer cylinder and the slower moving electrons impinge on the inner cylinder. Hence only those electrons enter the CMA whose energy is equal to the pass energy of the CMA. The pass energy of the CMA is the voltage difference between the inner and outer cylinders. The double pass design is intended to eliminate the background due to the secondary electrons generate within the analyzer. The negative voltage on the outer cylinder repels the electrons towards the openings on the inner cylinder to the electron multiplier inside it. The electron multiplier multiplies the signal by $\sim 10^{6}$ to10^{7} times to be measured by the channeltron. As the channeltron is a very delicate instrument, the output current has on both the K.E of the electrons and the repelling voltage applied, the greater the electron are repelled from the OC and attract towards the IC. The IC has slits to let electrons pass through. Hence, the voltages applied on the IC and OC

controls the K.E of the electrons. The pass energy and the energy of electrons to pass through the analyzer voltage applied to the terminals is

$E_{pass} \sim 1.7e(V_{IC}-V_{OC})$; E_{pass} is in eV and $V_{cylinder}$ is in (V) ; e - charge of the electron. If e=1 and V_{ic}, V_{oc} is in voltage E_{pass} will be in eV.

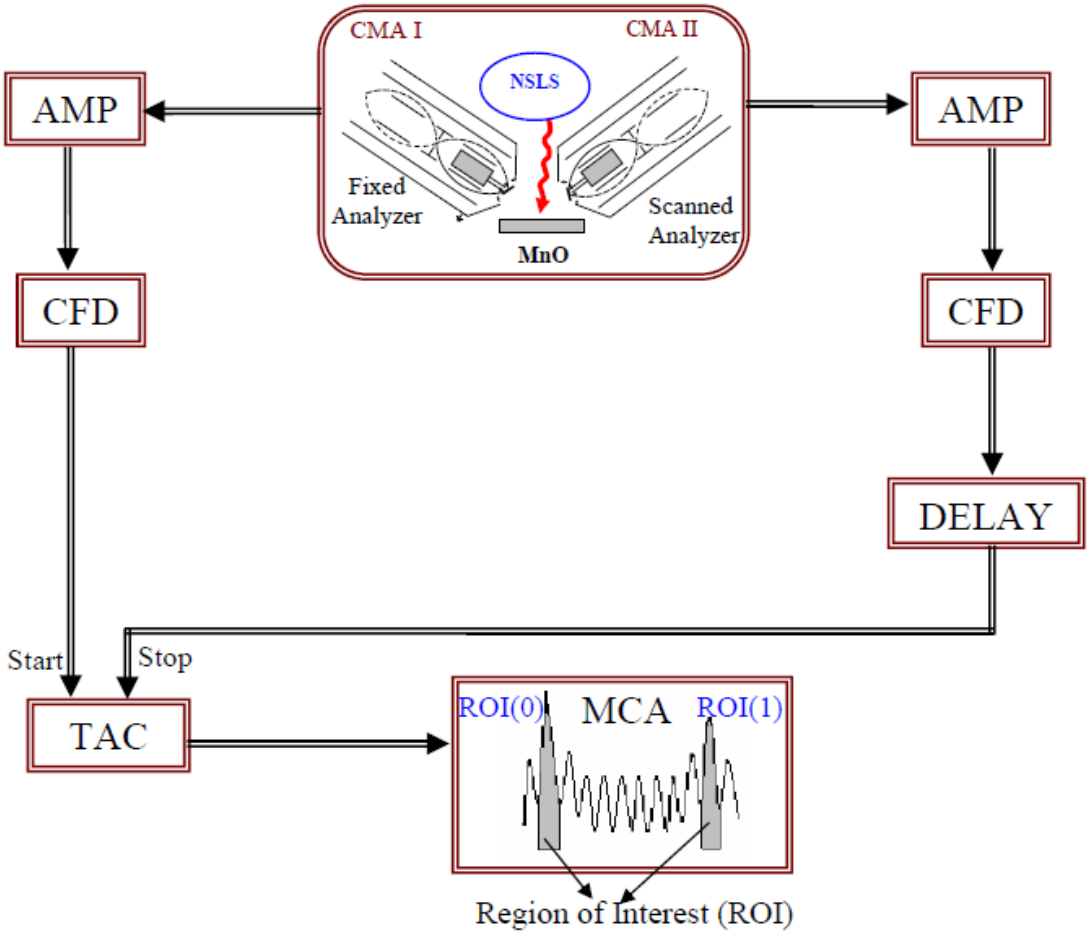

Fig. 2.9 Coincidence electronics [16](Ref 16, R. Sundaramoorthy, Thesis, 2007)

The hemispherical retarding grids and two cylindrical CMA's help us to achieve the required energy resolution. The larger aperture is used to obtain a greater area of acceptance which increases the count rate and leads to a better signal- to- noise ratio with a corresponding loss in energy resolution. The diameter of the aperture affects energy resolution and luminosity.

CMA modes: the CMA can be operated in retarding and non retarding modes. The CMA is operated in the retarding mode for this experiment. The electrons passes through (double –pass) two stage cylindrical mirror analyzer with their initial kinetic energy either accelerated or decelerated to obtain fixed pass energy. The retarding grid on the outer cylinder of the CMA provides the necessary acceleration and deceleration of the electrons. The energy resolution varies when the CMA is operated in a retarding mode; for the double pass cylindrical mirror analyzer with a point source, $\Delta E/PE$ is about 6% for small aperture and 16% for large aperture.

Coincidence Electronics: The schematics of the coincidence electronics is shown in Fig. 2.10. The output of the RCMA and LCMA is distributed to an amplifier and a discriminator. The output signal from the discriminator and the amplifier of one CMA is used as the start signal of a time to amplitude convertor. The signal from the second CMA which too is discriminated and amplified is sent to the delay so that the data is in the positive regime; this signal becomes the stop signal to the TAC. The output signal is the time difference between the start and stop pulse, the MCA records this pulse as a histogram.

2.6 Experiment Setup

The Fig.2.10 is the diagram of the experiment performed at the National Synchrotron Light Source (NSLS), Brookhaven National Labs (BNL). The samples used to perform the experiment are single crystals of Silver (Ag) and Copper (Cu). The samples are circular with a diameter of 10 mm and have a thickness of 5 mm. The two cylindrical mirror analyzers were used to analyze the emitted electrons from the sample. Coincidence events are considered only when both the photoelectrons and Auger electrons are detected at the same time at the respective analyzers. The time taken for an auger transition to occur is 10^{-15} s and the timing of the laboratory electronics is limited to 10^{-9} s, hence this allows us to determine that both the

electrons come from the same event from the same atom. The coincidence counts were measured by fixing one of the cylindrical mirror analyzers at a characteristic energy of interest in the photoelectron spectrum, while the second cylindrical mirror analyzer scans the corresponding auger spectrum. This generates the coincidence Auger spectrum. The samples were cleaned for approximately 40 minutes daily by sputter anneal techniques, until the photoemission spectra showed negligible evidence of impurities.

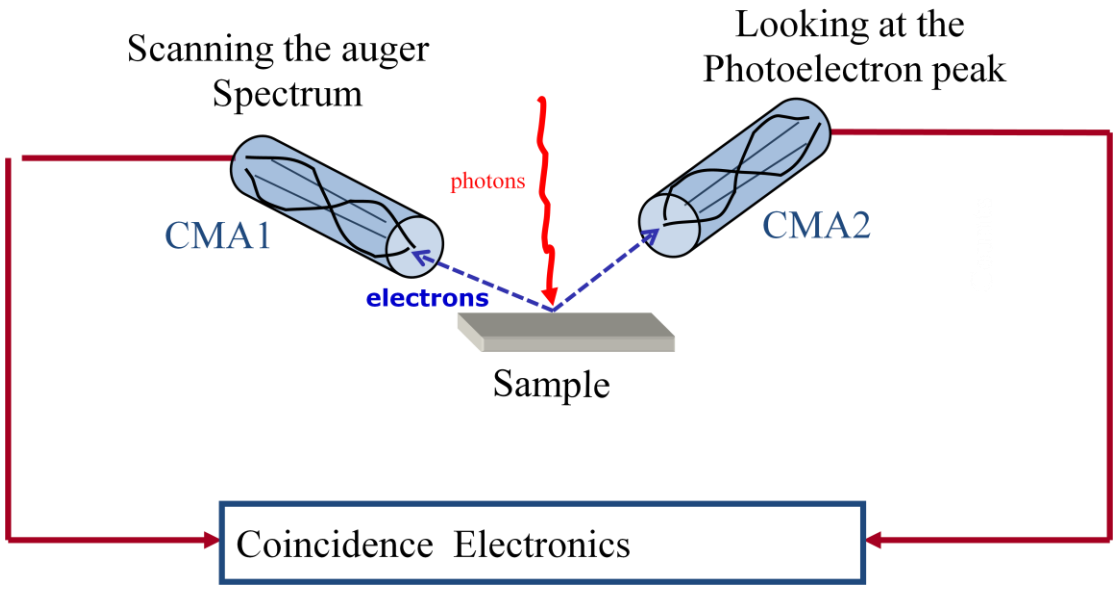

Fig. 2.10 Overview of the experiment setup. The CMA 1 scans the Auger spectrum, CMA 2 is fixed at the photoelectron energy.

CHAPTER 3

RESULTS AND DISCUSSION

3.*1 Results*

Fig.3.1 is a singles spectrum of Ag (100) with energy in electron volts (eV) along x- axis and counts along y - axis. A photon beam of energy hν = 185 eV is incident on the sample to generate a photoelectron spectrum. In this spectrum, we observe the valence band peak at 180 eV. From the Einstein's equation stated in chapter one, the 4p3/2 and 4p1/2 peaks are observed at ~120 eV. The binding energies for 4p3/2 and 4p1/2 core peaks are 63.7 eV and 58.3 eV respectively. The 4s core peak is seen at 87 eV. The binding energy is given by 97 eV. From the photoelectron spectrum it is evident that as we go lower in energy, the intensity of the signal increases. In order to identify the individual processes contributing to the Low Energy Tail of the spectrum, a coincidence spectrum is measured.

The Fig.3.2 is the spectrum of Ag (100) in coincidence with the 4p core peak, the coincidence counts are on the y - axis and the energy is on the x - axis. The left cylindrical mirror analyzer is fixed at 132 eV corresponding to the $4P_{1/2}$ core photoelectron energy. The Auger peak related to the photoelectron decay is seen at 40 eV. At energies lower than the Auger peak (0-40 eV), the Low Energy Tail (LET) of the spectrum is increasing with a broad maximum at roughly 20 eV. It is therefore important to understand the various contributions to the LET. To estimate the contribution to the Low Energy Tail due to the true coincidence with photo emitted valence band photoelectrons, we fix the left cylindrical mirror analyzer at 142 eV, 10 eV above the core photoelectron peak. The Einstein's equation prohibits the emission of an Auger electron as the valence band electrons leave the surface with energy greater than 132 eV and hence we do not see an Auger peak at 40 eV. The coincidence spectrum shown in Fig.3.3 is taken 10 eV above the Ag 4p photoelectron peak. As expected we see no Auger peak at 40 eV.

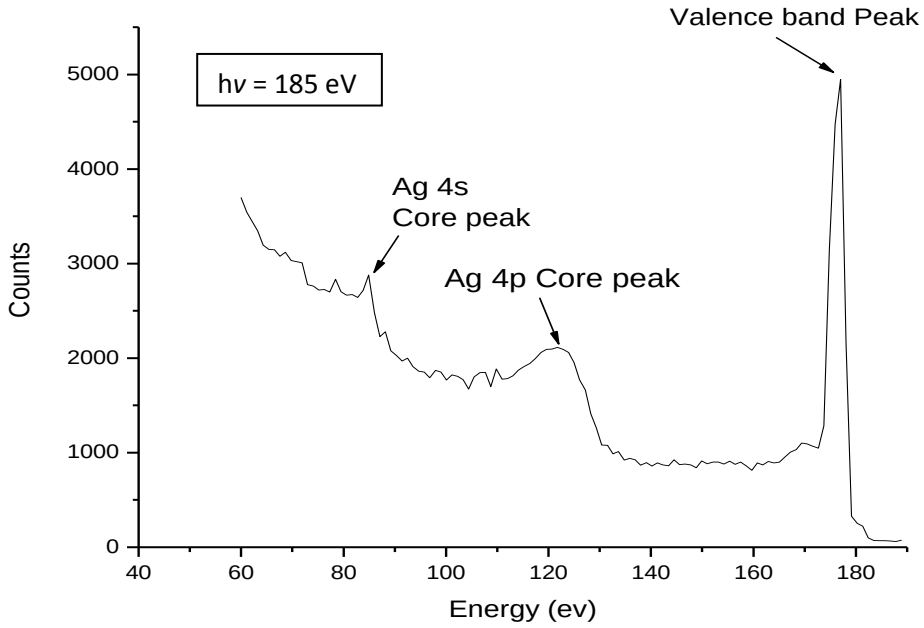

Fig. 3.1 Photoelectron Spectrum of Ag (100), incident by a photon of beam energy 185 eV with -5 V bias. The Ag 4p and 4s peaks are clearly visible at 120 and 87 eV respectively.

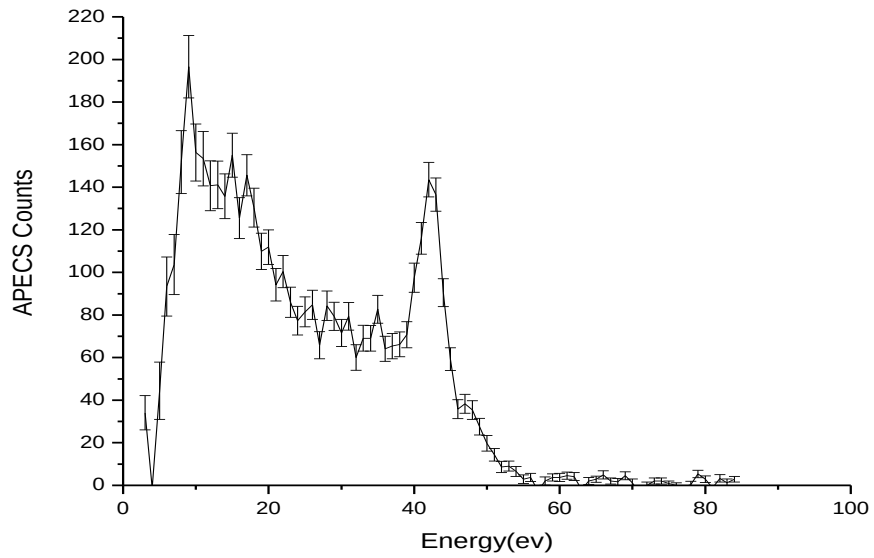

Fig. 3.2 Coincidence spectrum of Ag (100) with 4p photoelectron peak with -5 V bias. The Auger peak at 40 eV is clearly visible accompanied by a lot of spectral weight at lower energies below the Auger peak.

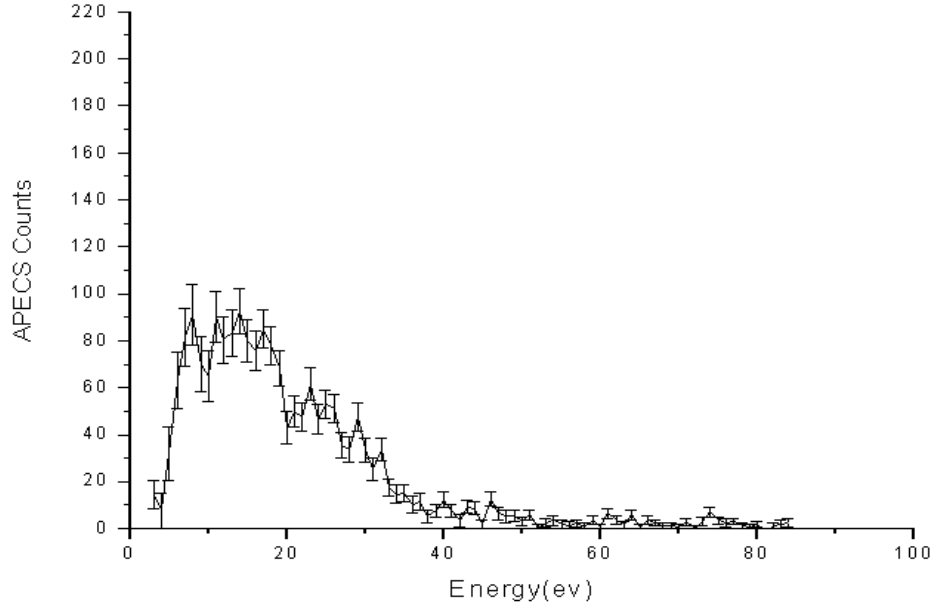

Fig. 3.3 Coincidence spectrum of Ag (100) 10 eV above the photoelectron peak with -5 V bias. The incident photon beam energy is 185 eV. The absence of the Auger peak is due to energy conservation of photoelectron.

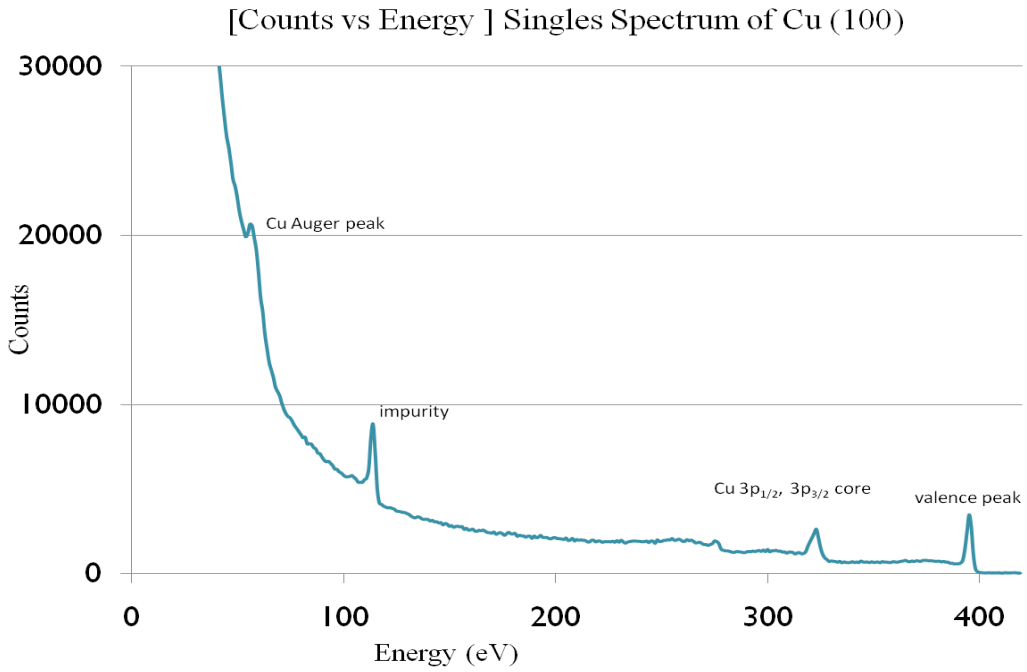

Fig. 3.4 Photoelectron spectrum of Cu (100) down to 0 eV with -5 V bias. A photon beam of energy 400 eV is incident on the sample, the $3p_{1/2}$ and $3p_{3/2}$ core peaks are visible at 320 eV. The Auger peak can be seen sitting on a large background at 60 eV.

Fig.3.4 is a photoelectron spectrum of Cu (100) single crystal. The energy in electron volts (eV) is along x-axis and the counts along y - axis. A photon beam of energy hν = 400 eV is incident on the sample to generate a photoelectron spectrum. The valence band peak is at 380 eV. The $3P_{1/2}$ and $3P_{3/2}$ core binding energies are given by 77.3 eV and 75.1 eV respectively. From the conservation of energy formula discussed earlier, the 3p1/2 and 3p3/2 core peaks are observed at 320 eV. The Auger peak is barely visible at 60 eV. A carbon impurity peak is also visible at 116 eV. The photoelectron spectrum of Cu (100) looks similar to that of Ag (100) with the spectral weight increasing at lower energies. Fig.3.5 is the spectrum of Cu (100) in coincidence with the $3p_{3/2}$ core peak, the coincidence counts are on the y - axis and the energy is on the x - axis. A photon beam of energy hν=220 eV is used to excite the $3p_{3/2}$ core electron. The left cylindrical mirror analyzer was fixed at 147.6 eV to detect the core electron excitation in Cu (100). The subsequent Auger transition related to the photoelectron excitation is seen at 60 eV. At energies lower than the Auger

peak (0-60 eV), the LET of the spectrum follows a similar trend as observed in Ag (100). We observe a broad maximum in the LET at roughly 20 eV. We repeat the experiment performed earlier on Ag (100) on Cu (100) to estimate the various contributions to the Low Energy Tail (LET) due to the valence band. We fix the left cylindrical mirror analyzer 10 eV above the $3p_{3/2}$ photoelectron peak. At this fixed energy the Einstein's equation prohibits the emission of an Auger electron by a phton beam of energy 200 eV. Hence we should not see an Auger peak at 60 eV. The left cylindrical mirror analyzer is now fixed at 157.6 eV, 10 eV above the $3p_{3/2}$ core peak and a coincidence spectrum measurement is run. The Fig.3.6 presents the data obtained. Consistent with previous experiments we see no Auger peak at 60 eV.

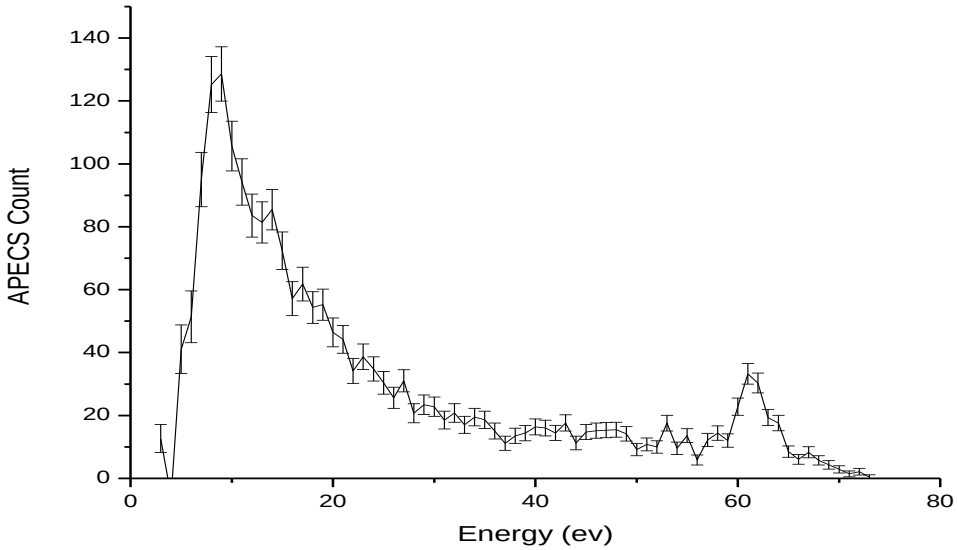

Fig. 3.5 Coincidence spectrum of Cu (100) with $3p_{3/2}$ photoelectron peak with -5 V bias. The photon beam energy is 220 eV. The photoelectron CMA is fixed at 147.6 eV. The Auger peak is visible at 60 eV. The Low energy Tail is visible at energies below the Auger peak with a broad maximum at 20 eV.

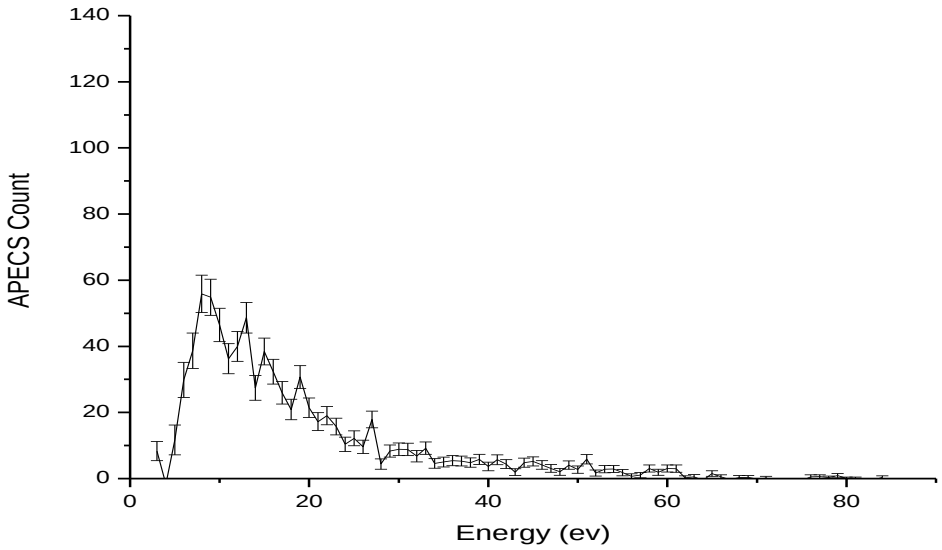

Fig. 3.6 Coincidence spectrum of Cu (100) 10 eV above the $3p_{3/2}$ photoelectron peak with -5 V bias. The photon beam energy is 220 eV. The photoelectron CMA is fixed at 157.6 eV. The Auger peak is absent at 60 eV.

3.2 Discussion

3.2.1 Origin of Low Energy Electrons

The various processes contributing to the low energy electrons for a given spectrum can be classified as intrinsic and extrinsic to the Auger transition. An intrinsic process can be explained as the generation of low energy electrons due to a direct consequence of the Auger transition. Similarly extrinsic process can be explained as the generation of low energy electrons due to indirect consequence of the Auger transition. The major contributions to the low energy electrons are

1. Inelastic tail of the valence band photoelectron peak.
2. Inelastic tail of the core photoelectron peak.
3. Inelastically scattered Auger electrons.

1. Inelastic tail of the valence band photoelectrons: The valence band contributes a large number of low energy electrons in a spectrum. The electrons in the valence band are loosely bound and hence need very little energy to escape from the sample surface. Hence when the photon beam is incident on the sample, the valence electrons are excited and escape out of the sample. The incident beam of photons excites the electrons in the valence band, the excited electron scatters inelastically with other valence electrons and the energy is shared by multiple electrons. The electrons on the way out of the sample contribute to the low energy background of the spectrum. In addition, there is a probability that the valence electrons escape the sample at energies equal to the photoelectron energies and appear in the spectrum, even though they do not contribute to the Auger process. In the photoelectron spectrum of Ag (100) and Cu (100) we observe the core photoelectron peaks sitting on a large low energy electrons contributed by the valence band. This contribution is extrinsic to the Auger mechanism and hence has to be removed. Since both the Auger and Photoelectrons are detected simultaneously in APECS and the energy of the photoelectron is less than the pass energy on the fixed cylindrical mirror analyzer, these electrons are not detected.

2. Inelastic tail of the core photoelectron peak: The first stage in an Auger mechanism is the knocking out of the core electron. This electron is also known as the photoelectron. The photoelectron on its way out of the sample can scatter inelastically with the valence electrons and in turn, distribute a part of its energy to valence electrons on its way out. The valence electrons after having gained sufficient energy from the expelled photo electron escape the sample surface and contribute to the low energy part of the spectrum. The photoelectron spectrum of Ag (100) shown in Fig 3.1 illustrates the contribution of the core photo electron peak to the low energy background of the spectrum. We can see that the Ag 4s core peak is sitting on a background contributed by the valence band. The Ag 4p peak is clearly visible to be sitting on a background due to the Ag 4s peak and the background due to the valence electron. This background can be eliminated by difference measurements.

3. Inelastic scattering of Auger electrons: Auger electrons may scatter inelastically and share their energy with one or more valance electrons. These electrons may leave the sample surface and end up in the LET part of the spectrum.

In addition to the above stated contributions, the electrons may have been scattered inelastically inside the cylindrical mirror analyzers. Measurements made by Jensen et al., revealed that these contributions are small and can be neglected when considering the other main processes responsible for the low energy spectrum.

3.3 Estimation of contributions to the APECS spectra from inelastically scattered VB photoelectrons

As discussed briefly above, the energy of the incident photon can be shared amongst several valence electrons either through inelastic scattering of a photo-emitted valence band electron as it exits the surface or through a direct multi-electron photoemission process[28]. In either case, the emission of multiple valence band (VB) electrons with energies in the range of the relatively flat LET below the VB photoemission peak could result in a true coincidence between and a VB photo-electron emitted in the range of the core electron photoemission peak and another valence band photo-electron emitted in the region of the LET of the Auger peak. In order to estimate the size of this contribution, coincidence measurements were made with the fixed analyzer set 10eV above the core. As a first approximation to eliminate the contribution from the valence band photoelectron, we performed a difference measurement. We subtracted the coincidence spectrum above the photoelectron peak from the coincidence spectrum with the photoelectron peak. This difference measurement is performed on Ag (100). The coincidence spectrum 10 eV above the 4p core peak Fig.3.3 is subtracted from the coincidence spectrum with the 4p core Fig.3.2. Fig.3.7 is the spectrum from the difference measurement; we still observe a lot of spectral weight below the Auger peak (40 eV). To estimate the contribution of the LET with respect to the Auger to the total spectrum, we calculate the area under the curve for the LET (i.e.) from 0 to 40 eV, this is done by adding the total counts from 0 to 40 eV. Similarly we calculate the area under the curve for the Auger peak. On dividing the areas under the curve

for the auger peak by the area under the curve for LET, we obtain a ratio of 2:1. We perform the difference measurement to Cu (100). The difference measurement is between the Cu $3p_{3/2}$ core peak and 10 eV above the core peak. The Fig.3.8 is the subtracted spectrum of cu (100). We again add the area under the curve of the LET from 0 to 60 eV and the area under the curve for the Auger peak. The ratio between the Auger peak and the LET is 1:6. The data analysis of Ag (100) and Cu (100) suggest that the Low energy Tail (LET) has contributions from processes intrinsic to the Auger transition.

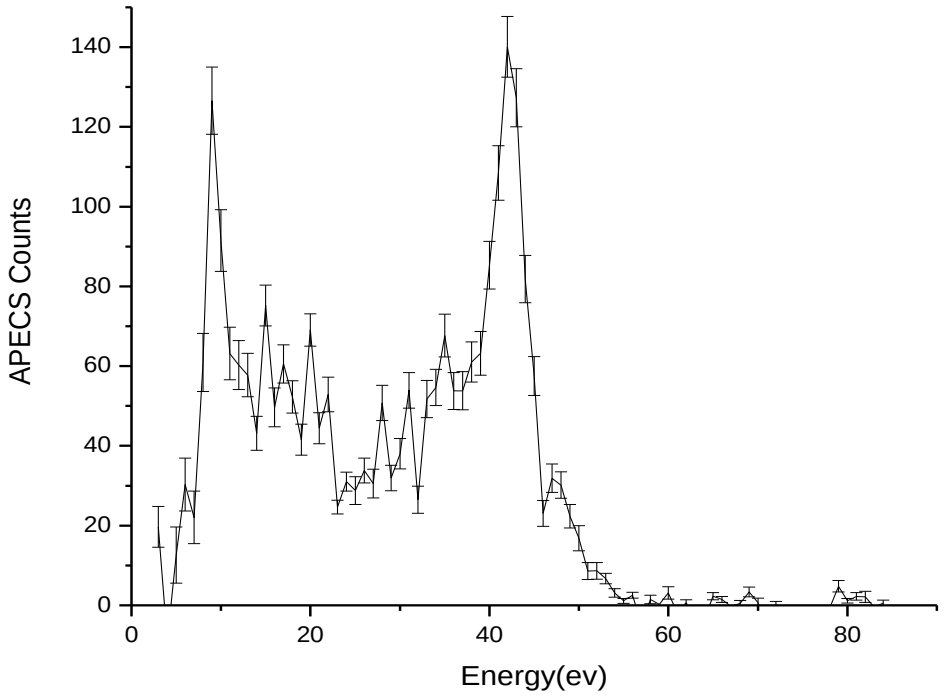

Fig. 3.7 Difference measurement coincidence spectrum of Ag (100) 4p Photoelectron peak with -5 V. The incident photon beam energy is 185 eV. The spectrum shows considerable spectral intensity at energies below the Auger peak (40 eV).

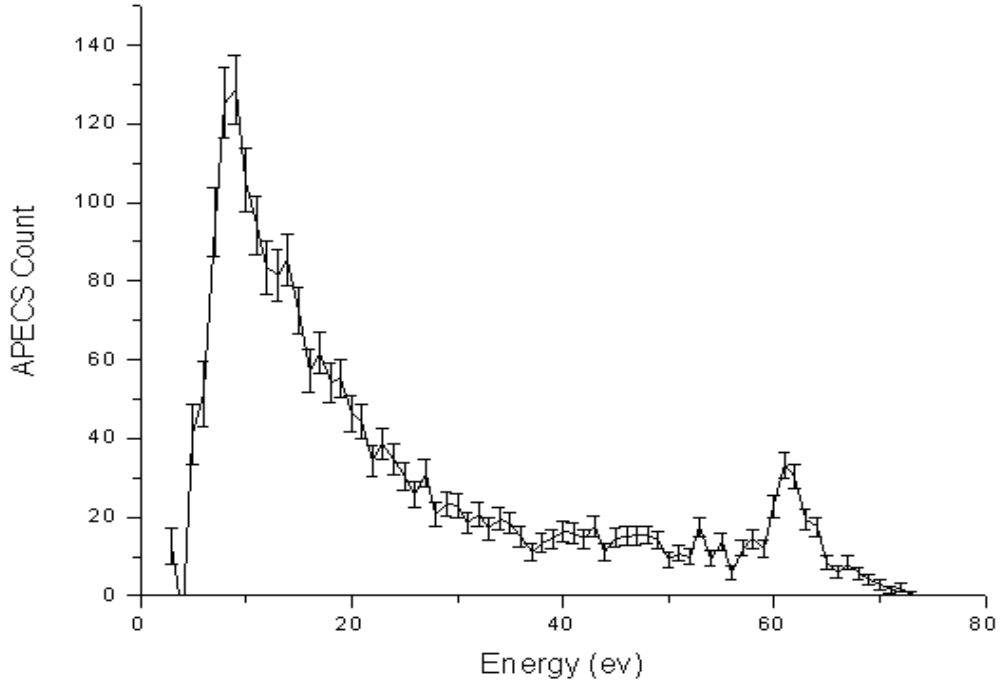

Fig. 3.8 Difference measurement of Cu (100) 3p3/2 photoelectron peak with -5 V bias. The incident photon beam energy is 220 eV. The spectrum shows considerable spectral intensity at energies below the Auger peak (60 eV).

3.4 Ramaker Function

S. Kalaskar, S.L Hulbert, B.R. Bartynski, A. H. Weiss[29] have pointed out that the contributions due to inelastically scattered VB photoelectrons can be expected to grow as the energy difference between the VB peak and the energy of the fixed analyzer increases. A photon beam of energy hv= 220 eV is incident on a sample exciting a valence electron; let's call this a photo emitted valence electron. The photo emitted valence electron loses energy inelastically to another valence electron. The energy equation is given by

$$K.E_{v1} = hv - E_{v1} - \Delta - Ø$$

In the above equation

$h\nu$ = energy of the photon beam.

E_{v1} = Binding energy of the valence electron.

Δ = energy lost to the second valence electron.

Ø = Work function of the sample.

The energy of the second valence electron is given by the energy equation

$$K.E_{v2} = \Delta - E_{v2} - Ø$$

Tofacilitate estimation of the contribution from the inelastically scattered valence electrons to the LET and to extract the Auger lineshapes from the experimental data. A background function is assumed based on Ramaker's equation[26]. The overall background is given by:

The values A, B, C, E_0, m and n are constants generated by iteration methods using Origin software. Δ is calculated based on the photon beam energy and the energy at which the photoelectron CMA is fixed at. The incident photon beam energy on Cu (100) is 220 eV. The Photoelectron analyzer is fixed on 158 eV. The work function of the metal is 5 eV. The quantity 'Δ' therefore is given by 60 eV. The value of delta is used in the Ramaker's function to generate a mean square fit that fits 2/3rd of the data points in Fig.3.6. Fig.3.10 shows the Ramaker fit to the coincidence photoelectron data fixed at 157 eV. We can clearly see

the cut off at 60 eV. The values obtained from the fit and extrapolate it to Δ= 80 eV, as shown in Fig.3.11. The extrapolation function for Δ= 80 eV was subtracted from the coincidence spectrum with the $3P_{3/2}$ core peak. The resulting spectrum is shown in Fig.3.12. The relative contributions from intrinsic and extrinsic process were obtained by taking the ratio of the areas under the LET region and the Auger peak. The ratio between the LET and Auger peak is 7:1. This strongly suggests that a significant part of the LET is due to intrinsic processes associated with the Auger mechanism.

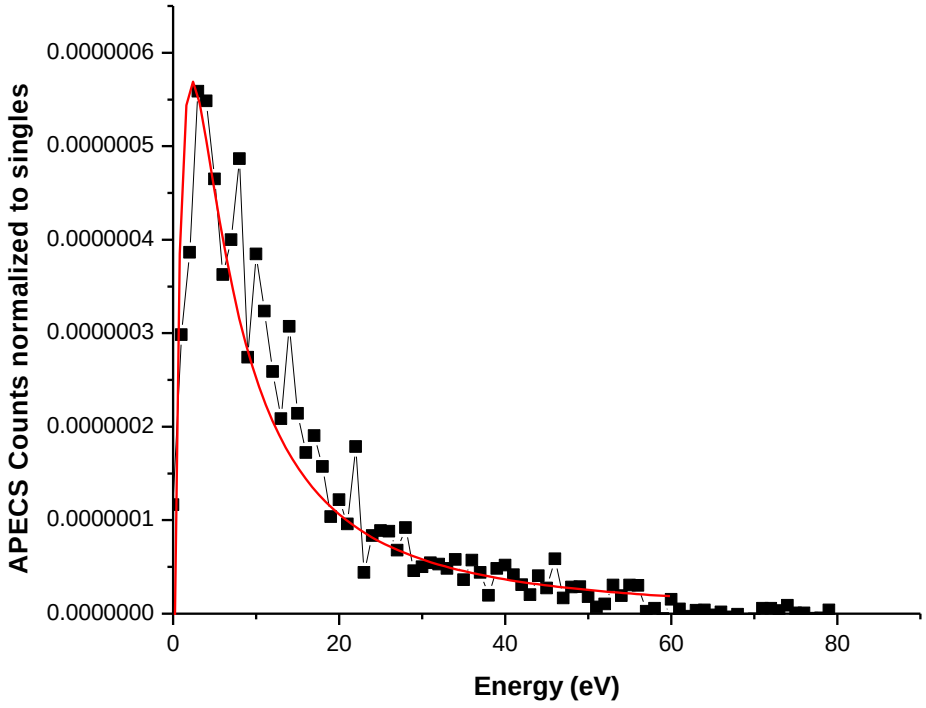

Fig. 3.9 Ramaker's function at Δ= 60 eV fit to the Coincidence data with 157 eV of Cu (100). The red line is the Ramaker's function generated using Origin software.

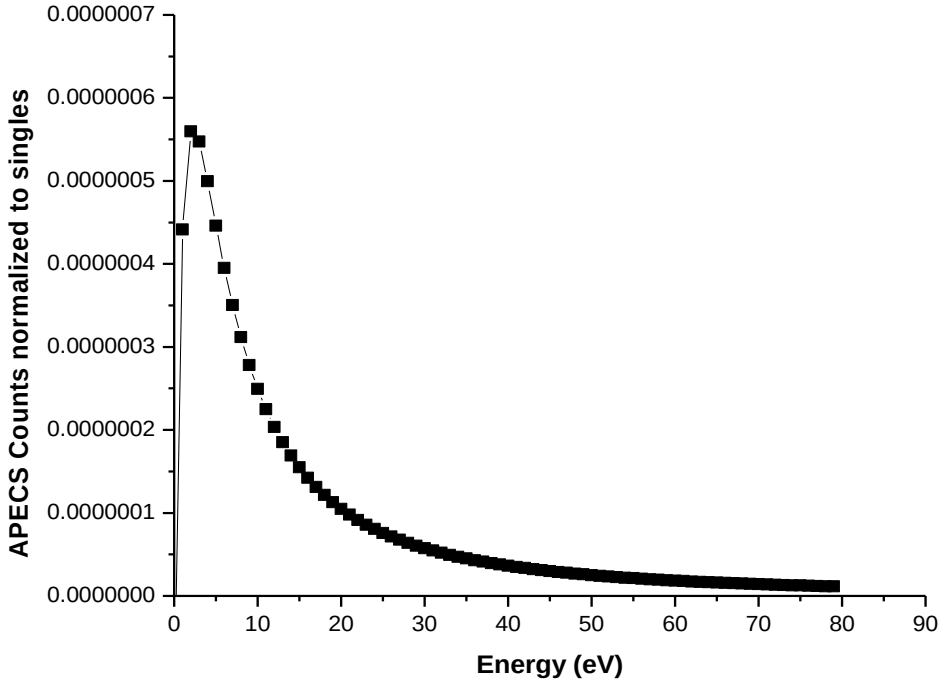

Fig. 3.10 Ramaker's function extrapolated to Δ= 80 eV using the 60 eV data of Cu (100).

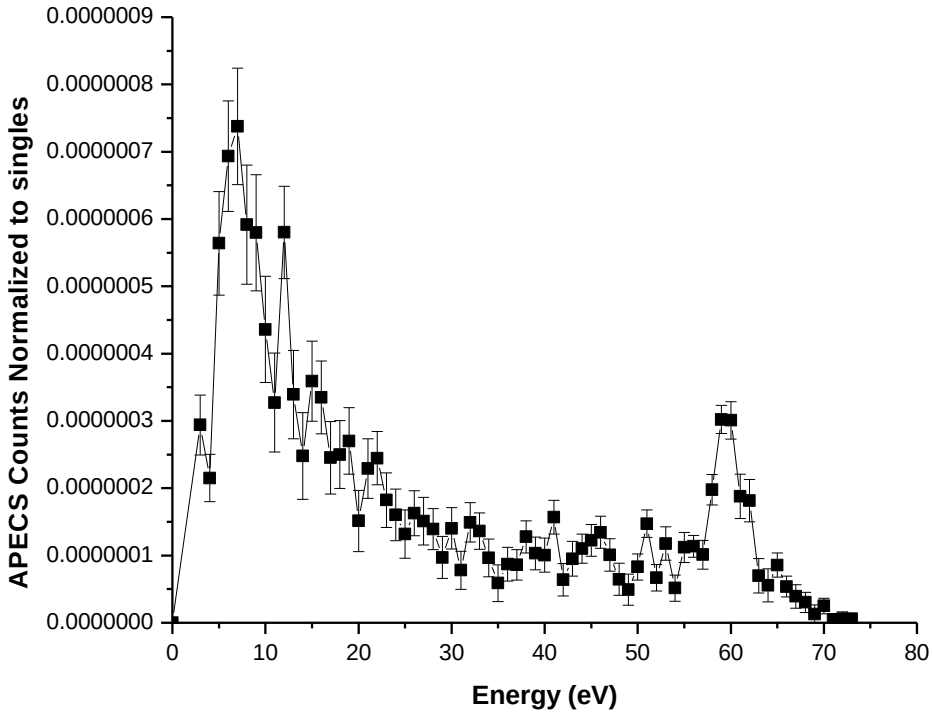

Fig. 3.11 Background free spectrum of Cu (100) in coincidence with $3P_{3/2}$ core.

3.5 Estimation of intrinsic and extrinsic contributions to the LET Spectrum

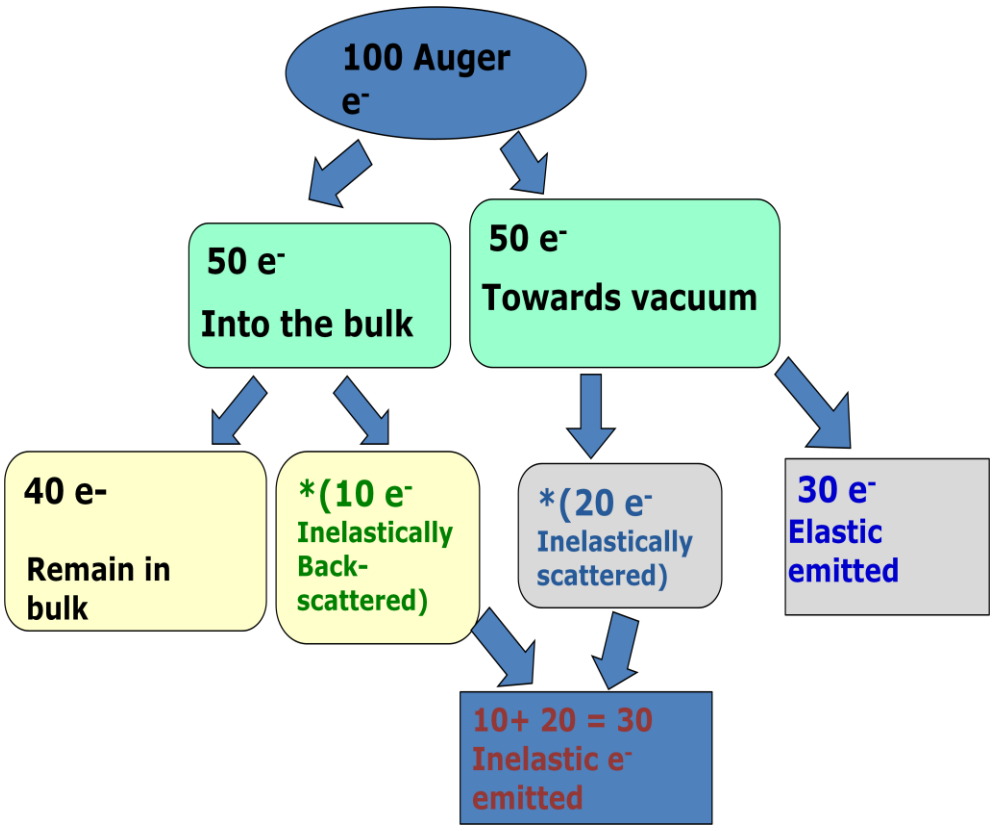

Fig. 3.12 Flow chart of the estimated contribution to the Low Energy Tail (LET) due to scattering of Auger electrons on the way out of the sample. The ratio is in terms of elastically and inelastically scattered Auger electrons.

To estimate the intrinsic and extrinsic contributions to the LET of a given spectrum, let us consider that at any given time during the experiment there are 100 Auger electrons emitting out of the sample. Of these 100 Auger electrons, 50 electrons go into the bulk and 50 travel towards vacuum. The 50 electrons that travel into the bulk, 40 electrons remain in the bulk and 10 electrons are inelastically back-scattered as shown by Lin et.al [25]. Of the 50 electrons travelling towards vacuum, 20 electrons are scattered inelastically out of the sample as shown by Jensen et.al and the remaining 30 electrons are scattered elastically on their

way out of the sample. On comparing the contributions to the LET, we see that the ratio of intrinsic to extrinsic contributions is given by 1:1. The Fig.3.9 illustrates the estimation in a flowchart.

3.6 Conclusion

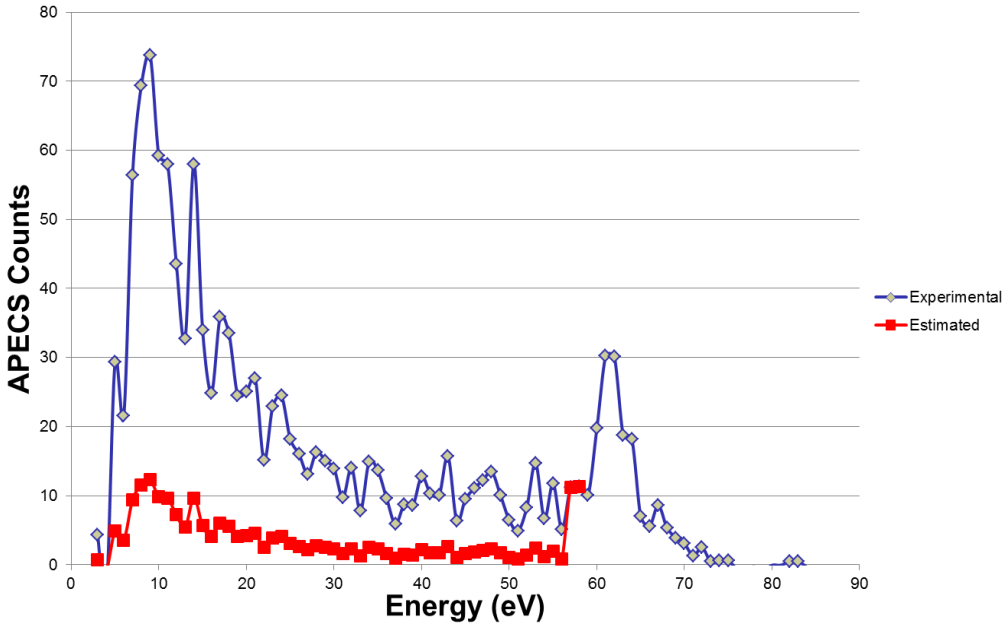

Fig. 3.13 Spectrum showing the comparison between Experimental vs. Estimated values for the Low Energy Tail (LET) in Cu (100). The blue graph is the experimental curve and the red graph is the estimated curve.

The Fig.3.13 and Fig.3.14 present the comparison between experimental and estimate of the LET part of the spectrum based on the analysis discussed in section 3.5 in Cu (100) and Ag (100) respectively. On comparing the estimated values with the experimental values it is clear that the processes shown in Fig.3.12 are not sufficient to account for the LET. The Auger mechanism does not decay by a single electron emission alone, but the energy made available due to the filling of the core hole is shared by multiple Auger electrons. In this case, the Auger final state is not a two valence hole, one electron state, but a n-valence hole, n-1 electron state with n>2.

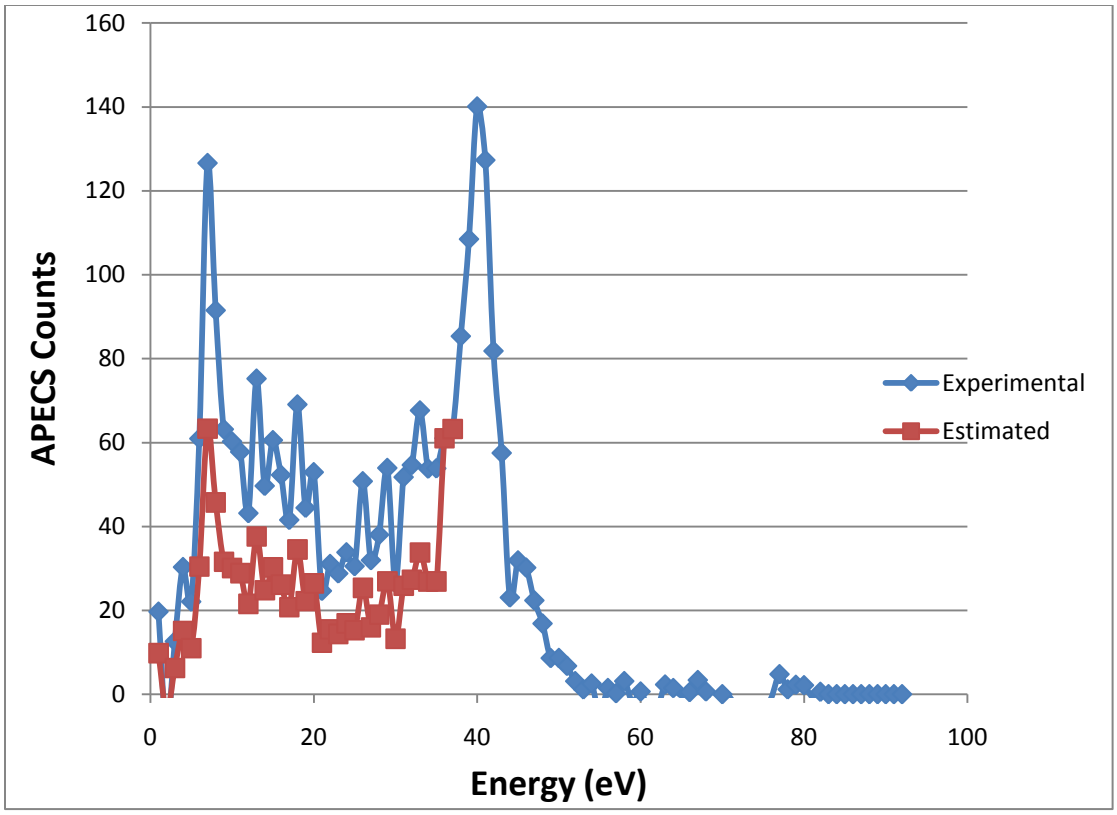

Fig. 3.14 Spectrum showing the comparison between Experimental vs. Estimated values for the Low Energy Tail (LET) in Ag (100). The blue graph is the experimental curve and the red graph is the estimated curve.

CHAPTER 4

SUMMARY

We have presented measurements in which the Auger Photoelectron Coincidence Spectroscopy (APECS) technique was used to probe energy distribution of electrons emitted as the result of $N_{2,3}$ VV and $M_{2,3}$ VV Auger transition in Ag (100) and Cu (100) respectively over a full range of emitted energies from 0 eV to 81eV. The experiments reported in this thesis were carried out at the National Synchrotron Light Source (NSLS), Brookhaven National Labs (BNL), Upton, New York. A variable synchrotron radiation in the UV range was used to excite the samples under investigation. Two cylindrical mirror analyzers (CMA) were used to detect the photo electrons and the auger electrons. The right CMA was fixed on the photoelectron core peak and the left CMA used to scan the corresponding auger energy range. Photon beam of energies 185 and 220 eV impinged on Ag (100) and Cu (100) respectively. A coincidence spectrum was taken with the right CMA fixed on the 4P core peak in case of Ag (100) with the fixed cylindrical mirror analyzer fixed at 132 eV and $3P_{3/2}$ core peak in case of Cu (100) with the fixed cylindrical mirror analyzer is fixed at 147.6 eV, while the left CMA scans the corresponding Auger energy range. In order to estimate the contributions to the low energy spectrum due to processes extrinsic to the auger transition, a coincidence spectrum was taken 9 eV and 10 eV above the 4P and $3P_{3/2}$ core peak for Ag (100) and Cu (100). To eliminate the extrinsic background contribution to the 4P and $3P_{3/2}$ core peak spectrum a difference measurement was performed by subtracting the valence band spectrum from the 4p and $3p_{3/2}$ core peak coincidence spectrum of Ag (100) and Cu (100) respectively.

The coincidence measurements were successful in separating the low energy Auger lines from a large background, arising from loss processes unrelated to the Auger transition. The measurements have revealed a well formed Auger peak at 60 eV for Cu (100) and an Auger peak at 40 eV for Ag (100) accompanied by a low energy tail (LET) associated with $M_{2,3}VV$ transition. The Low Energy Tail (LET) extends to 0 eV and has a broad maximum at 6eV in case of Cu (100) and 10 eV in case of Ag (100). The integrated

intensity of the Low Energy Tail (LET) in Cu and Ag were 6 and 2 times larger than that of the Auger peak itself respectively. The origin of the LET is discussed in terms of extrinsic mechanisms in which electrons from the peak lose energy as they propagate to the sample surface, as well as intrinsic mechanisms in which multi-electron Auger processes distribute the energy gained by the filling of the core-hole to multiple valence electrons. The analysis of the spectrum reveals a lot of spectral weight in the low energy side of the spectrum. The integrated intensity of the LET is calculated by summing the total counts under the curve for the region below the Auger peak down to 0 eV. The ratio between the total counts under the LET and Auger peak gives us 2:1 and 6:1 in case of Ag (100) and Cu (100) respectively. To better estimate the contributions from the valence band to the background, a modified Ramaker function is used to fit the coincidence data at 10 eV above the 3P3/2 core in Cu (100). The given result is used to extrapolate the value to 80 eV and subtracted from the $3P_{3/2}$ coincidence spectrum in Cu (100). The ratio between the LET and the Auger peak is 7:1, which is similar to the Coincidence spectrum of Cu (100) obtained from direct subtraction. An estimate based on known extrinsic processes indicates that the ratio between the LET and the Auger peak should be close to 1:1. Comparing the estimated values with the experimental values is clear that the processes shown in Fig 3.12 are not sufficient to account for the LET. The Auger mechanism does not decay by a single electron emission alone, but the energy made available due to the filling of the core hole is shared by multiple Auger electrons. In this case, the Auger final state is not a two valence hole, one electron state, but a n- valence hole, n-1 electron state with n>2.

REFERENCES

(1) M.P Auger, Compt, Rend 180, 65 (1925).
(2) V. Schmidt et.al, PRL, 38, 63, 1977.
(3) Atomic, Molecular and Optical Physics, 28 (1995) 1761.
(4) Auger Photoelectron Coincidence Spectroscopy in Cu- H.W. Haak, G.A. Sawatzky, T. D. Thomas, PRL, Vol.41, No.26 (1978).
(5) Auger Photoelectron coincidence Spectroscopy- S.M. Thurgate, Aust. J. Phys., 43, (1990).
(6) Review of Photoelectron Spectroscopy – John l. Pobins , Vol.48, Nos 1-4, (1995).
(7) APECS using Synchrotron Radiation- R. A. Bartynski, E. Jensen, S.L.Hulbert, C.C.Kao, Progress in Surf Sci, Vol 53, Nos. 2-4, pp. 155-162,(1996).
(8) Enhanced sensitivity to oxide surface defects using Auger Photoelectron Coincidence Spectroscopy- A.K. See, W.K. Siu, R.A. Bartynski, A. Nangia, A.H. Weiss, S.L. Hulbert, X. Wu, C.C. Kao, Surface Science 383, (1997).
(9) "Coincidence Ti 3p Core Level Photoemission Spectra from NH 3 Covered TiO 2(110) Surfaces," W. - K. siu, A.-K. See, R.A. Bartynski, A. Nangia, A.H. Weiss, Xilin Wu, S.L. Hulbert, March Meeting, APS (1997).
(10) "The anomalous line shape of the Pd M_45VV Auger spectrum in dilute Pd/Ag(100) surface alloys resolved by APECS," D.A. Arena, R.A. Bartynski , R. Nayak, A.H. Weiss, S.L. Hulbert, March Meeting of the APS, March 12-16,Seattle, Bull. Amer. Phys. Soc. 46 (2001).
(11) Giant Coster-Kronig transitions and intrinsic line shapes of the anomalous Pd $M_{45}VV$ Auger spectrum of Pd/Ag (100) dilute surface alloys, D.A. Arena, R.A. Bartynski, R.A. Nayak, A.H. Weiss, S. L. Hulbert, Michael Weinert, Phys. Rev. Lett. , 91, 176403 (2003).
(12) "Modeling of LMM-MVV Auger-Auger Coincidence Spectra From Solids," R. Sundaramoorthy, A.H. Weiss, S.L. Hulbert, and R.A. Bartynski, Bull. Amer. Phys. Soc. 51 (2006).
(13) Direct evidence for dynamic broadening of the energy spectra associated with the later steps of an Auger cascade, R. Sundaramoorthy, A. H. Weiss, S. L. Hulbert, and R. A. Bartynski, Phys. Rev. Letts. PRL 101, 127601 (2008), doi:10.1103/PhysRevLett.101.127601
(14) Origin of the low- energy tail in the Al $L_{2,3}VV$ Auger spectrum studied with Auger-photoelectron coincidence spectroscopy- E.Jensen, R.A. Bartynski, R.F. Garrett, S.L. Hulbert, E. D. Johnson, C.-C. Kao.
(15) Practical Surface Analysis- D. Briggs and M.P. Seah, Vol 1, (1983).
(16) R.Sundaramoorthy, Thesis, 2007.
(17) Herman Winick and Doniach- Synchrotron Radiation Research.
(18) Rob Z. Bachrach, Synchrotron Radiation research (1992).
(19) NSLS control room-LINAC, booster, RF notes.
(20) www.nslsbnl.gov/about/imagelib/images/lr/beamline-status-lowres.jpg.
(21) S.L. Hulbert, J.P. Stot, F.C. Brown,N.C.lien, Nucl. Instrum, 1 208, 43, (1983).
(22) PES experiment control program users manual-R.F. Garrett, J. Lepreyesh and S.l. Hulbert, BNL 43886 (1990).
(23) C.Gahiwiller and F.C. Brown, PRB 2, 1918 (1970).
(24) PHI Model 15-255G Cylindrical Mirror Analyzer manual.
(25) Y. Lin and D.C. Joy, Surf Interface Anal. 2005; 37:895-900.
(26) D.E. Ramaker, J.S. Murday and N.H. Turner, elec. Spec., 17, 45-65, (1979).
(27) http://www.nsls.bnl.gov/beamlines/beamline.asp?blid=U1A.
(28) Direct and core-resonant double photoemission from Cu (001)- grant van Riessen, Zheng Wei, Rajendra S Dhaka, Carsten Winkler, Frank o Schumann and Jurgen Kirschmer, stacks.iop.org/JphysCM/22/092201.
(29) S.Kalaskar, Thesis,2010

BIOGRAPHICAL INFORMATION

Karthik Shastry received his Master of Science degree in Physics from Vellore Institute of technology in 2010. Then he moved to University of Texas at Arlington in Fall 2007 as a masters student in Department of Physics. He completed his Masters in 2010 with dissertation titled "First Measurements of the Low Energy Tail (LET) down to 0 eV Using Auger Photoelectron Coincidence Spectroscopy (APECS) in Ag (100) and Cu (100)". He is currently pursuing his PhD studies at the Dept of Physics, UTA.